GEO 511 Master's Thesis

Where does it come from, Where does it go?

An Integral Assessment of the Supraglacial Debris Cover of Zmuttgletscher, Swiss Alps

Author:
Rahel Ganarin
rahel.ganarin@geo.uzh.ch
12-737-722

Supervisor:
Nico Mölg
nico.moelg@geo.uzh.ch

Supervisor:
Dr. habil. Tobias Bolch
tobias.bolch@geo.uzh.ch

Supervisor and Faculty Member:
Prof. Dr. Andreas Vieli
andreas.vieli@geo.uzh.ch

30th September 2018
Department of Geography, University of Zurich

Preface

I would like to thank my main supervisor, Nico Mölg, for the initial ignition of this project. Your input in our numerous discussions has been a great support throughout the course of this thesis.

Andreas Vieli infected me with his enthusiasm for glaciology in my very first semester of study. He taught me a large part of my knowledge in glaciology and geomorphology and thereby laid the foundation stone for this work. This thesis has been a great challenge for me, as it is highly conceptual. Thank you, Andreas, for your encouraging inputs during our meetings and for making time for me whenever I needed it.

I want to thank Tobias Bolch for his expert input during our talks. Your constructive feedback and your helpful literature recommendations were highly appreciated.

I thank Stephan Gruber for his support via Skype and email whenever I needed it for my work with his model. Your prompt responses were very welcome in times of need.

I deeply appreciate all the support I received from several researchers and employees at GIUZ: James Ferguson, for his «trademark skill of nodding» and for providing me with helpful literature. Oliver Burkhard, who helped me with a plotting challenge in R, and whose solution took him half an hour to come up with after I had been struggling for ten. Alessandro Cicoira, whom I learned so much from in terms of academic writing during our intense and fun ERTm project on Svalbard in 2018. Annina Brügger, for her great help with my conference abstract, for her valuable paper recommendations and for her always open office door. Manuel Bär, who meticulously proof-read some of my chapters and gave great input from a different perspective. And Isabelle Wüest, who never grew tired of answering my many administrative questions. «Sonnengruss» to you!

A massive thank you goes to my friends: For letting me go on and on about my thesis when it was going well and for hugs and dances and wine when it was not.

And last, but by no means least, I want to thank my parents, Siro and Susanne. You have supported me for as long as I can remember with your interest in what I do and your love. Thank you for teaching me to always try to give my best in everything I do. And to my family in general, for always nodding and smiling when I enthusiastically went on about «Schuttbedeckung» yet again. You guys are my rock. My debris, so to speak.

Abstract

Glaciers all over the world lose mass due to climate change. However, retreating glacier tongues are not the only pressing reaction that glaciers show to global warming. Supraglacial debris covers spread with increasing temperatures, due to a variety of reasons. Such sediment mantles alter glacier dynamics and melt behaviours to an extent that has not yet been fully captured. Given their increasing number and their widespread range of responses to climate change, debris-covered glaciers pose a crucial research topic in glacier monitoring and modelling.

Supraglacial debris covers are a function of the debris origin and deposition and the debris transport away from the input location. Therefore, debris mantles must be assessed integrally to captivate the whole framework of factors influencing and controlling them. To the best of my knowledge, this thesis poses the first study conducted so far to pursue such a holistic approach combined with numerous debris thickness field measurements in a case study. I conduct my research on Zmuttgletscher, a debris-covered valley glacier in the western Swiss Alps, which is regularly fed by avalanches entering debris into the glacial system. To assess the supraglacial debris cover, I make use of orthorectified aerial imagery, elevation data and ice flow velocity data for the glacier tongue. During a field measurement campaign, we collected 207 thickness measurements on the glacier tongue, yielding 121 measuring points with information about their surface topography and small-scale variability. For the quantification of debris origin and deposition, I mapped 28 avalanche deposition cones all along the headwall and combined their erosion input from the rock walls with the glacial flow units of Zmuttgletscher. This division of the glacier allowed me to associate debris thickness measurements on the glacier tongue with the deposition cones up-glacier. The flow units determined by the debris colour bands well match the flow velocity vector field, while the surface topography does not reproduce the trajectories, presumably due to the topography inversion effect. Established observations for supraglacial debris covers are met by my analyses, such as increasing thicknesses downglacier, decreasing emergence rates and the independence of slope and topography exposition due to the topography inversion effect. New site-specific observations are the debris thickness dependence on the aspect in relation to ice flow or debris melt out due to an icefall.

I conclude that the local topography and climate strongly influence supraglacial debris mantles. While being confined to the study area, the results and observations in this study still help to better understand the influence of supraglacial debris on glacier melt and dynamics.

Contents

List of Figures

List of Tables

x

1. Introduction

Glaciers, vast bodies of ice and rock, somehow caught in a perpetual loop of formation and disintegration, slowly flowing to their points of no return. Captivating formations of debris, snow, crevasses and awe-inspiring tongues. Having licked their immediate surroundings clean, they are now subtly musing at our belated attempts of mitigating climate change by sticking said tongues out of alpine valleys, ever with decreasing prominence. Glaciers have been a cool poster-child of environmental groups and scientists alike in discussions of global warming and the direct and indirect affect of these, but how do glaciers actually work? What drives them, flows them, builds them up, melts them down? Many of these questions have been answered in the uncountable amount of literature regarding the topic. Nevertheless, glaciers still harbour a few unsolved mysteries, one of which I will try to uncover throughout this thesis, where I broach the inconspicuous wallflower of glaciology: debris.

First, let us address the obvious first question when dealing with glaciers: What exactly is a glacier? Dobhal (2011) defines it as a dynamic ice body always moving downslope under the gravitational force of its own weight. It is characterised by two basic components: the accumulation and the ablation area, which are defined by the glacier mass balance. The *mass balance* of a glacier is the sum of all processes that add mass to a glacier and remove mass from it (Haeberli, 2011). Mass increase happens via direct precipitation in form of snow and subsequent firnification, via wind transport of snow or by snow and ice avalanching onto the glacier. Mass loss occurs via a variety of processes including melting and runoff, sublimation, evaporation, calving and wind transportation of snow out of a glacier basin. The *accumulation area* describes the higher elevated part of a glacier and marks the area where the annual mass balance is positive, i.e. mass gain exceeds mass loss. The accumulation area extends between the bergschrund, the crevasse between stagnant and flowing glacier ice, and the equilibrium line altitude (ELA). The *ELA* represents the zone where annual accumulation and ablation are equal (Bakke and Nesje, 2011). The *ablation area* extends between the ELA and the terminus of a glacier. It is the area where the annual mass balance is negative. The lowest part of the glacier is often referred to as glacier tongue or snout.

Glacier mass balance is a function of climate forcing and a direct, undelayed response of a glacier to the prevailing climatic conditions (Haeberli, 2011). Hence, it constitutes a key indication of climate change. Glaciers strive for a state of equilibrium, and in a warming climate, they retreat into higher elevated surroundings. With this dynamic response to a climate warming –
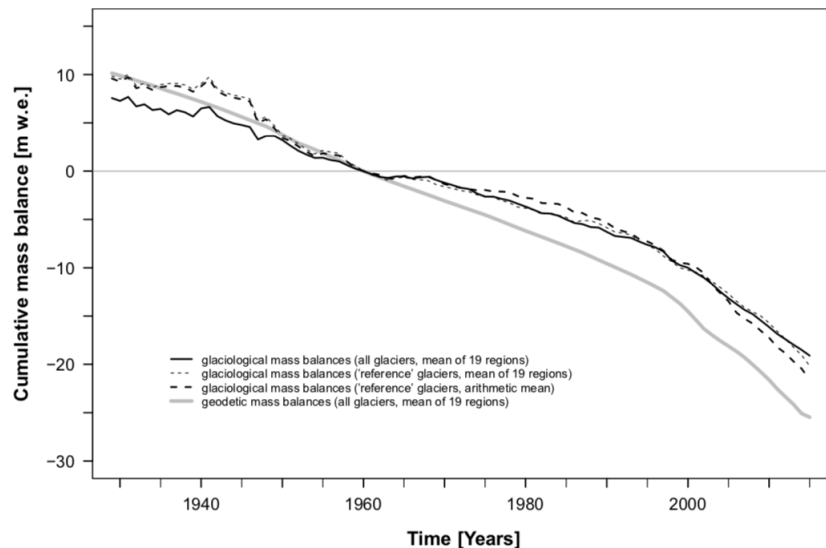
Figure 1. Global averages of observed cumulative glaciological mass balances and cumulative geodetic mass balances from 1930 to 2015, relative to 1960 (WGMS, 2017).

reduction in area mainly through the retreat of glacier tongues –, glaciers re-adjust their extent to equilibrium conditions of ice geometry with a zero mass balance (WGMS, 2017).

The Intergovernmental Panel on Climate Change (IPCC, 2014) states in his Fifth Assessment Report that the globally averaged combined land and ocean surface temperature has increased by 0.85 ± 0.2 °C between 1880 and 2012, and will continue to rise for all investigated future climate scenarios. The World Glacier Monitoring System (WGMS, 2017) has shown that, as a consequence of the increasing air temperatures, glaciers all over the world have had negative mass balances for decades and thus are losing ice mass. Figure 1 impressively illustrates this development and even delineates an acceleration of global ice mass loss since the late 1990's. Shrinking glaciers pose great problems all over the world, as they contribute to global sea level rise and alter the regional-scale water balance (IPCC, 2014).

1.1. Debris-covered Glaciers

1.1.1. Formation

A warming climate not only affects the glacial melt rates and mass balance, but also favours the formation of supraglacial debris cover on glacier tongues (e.g. Haeberli et al., 1997; Benn et al., 2012; Kirkbride and Deline, 2013). According to Kirkbride (2011), a debris-covered glacier is defined as a glacier with continuous debris cover across its full width on parts of the ablation area. Debris is defined as unconsolidated sediment with grain sizes larger than 1 mm (Bolch, 2011). Supraglacial debris covers form where debris supply is high, ablation is high and ice flow is slow (Anderson and Anderson, 2018). This results in the glacier being unable to evacuate rock debris efficiently. Therefore, debris mantles develop mostly on the lower parts of ablation zones on glaciers surrounded by steep rock walls.

Climate change has a primary effect on debris cover extent: Debris mantles expand globally because of rising temperatures (e.g. Kirkbride, 1993; Deline, 2005; Garg et al., 2017). Global
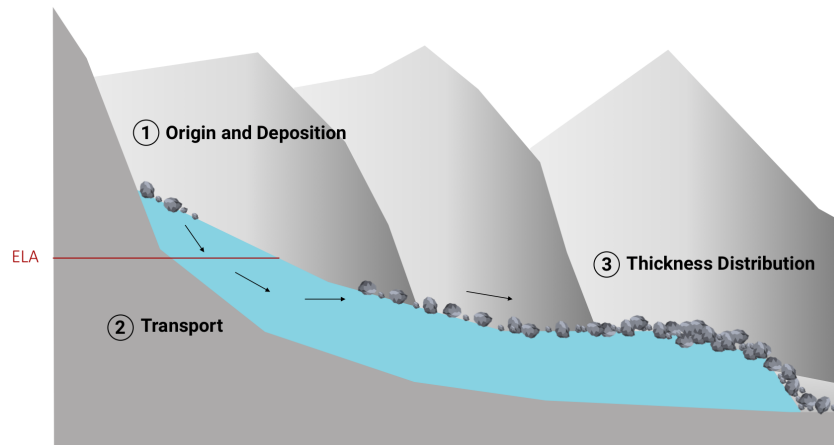
Figure 2. Conceptual model of the formation of a supraglacial debris cover. The red line marks the ELA. Black arrows show the sediment transport.

warming is known to lead to permafrost thawing, which affects the stability of steep slopes and causes increased weathering and hence more available debris (Hambrey et al., 2008). Debuttressing effects of missing ice masses and more exposed moraines also enter more debris into the system. Rather than receding in the manner normal to most alpine glaciers, debris-mantled glaciers undergo downwasting, where the surface subsides (Anderson and Anderson, 2016, 2018). A thicker cover of debris towards the terminus retards ablation more than the progressively thinner cover up-glacier. This results in a lessening or even reversal of the surface gradient, typically to less than 2° (Hambrey et al., 2008). All these effects result in an increasing number of glaciers becoming debris-covered on their ablation area. In addition, pre-existing debris covers are spreading up-glacier towards the ELA because of the greater ablation and slowing of ice above the upstream margin of the continuous debris cover (e.g. Kirkbride and Warren, 1999).

The spatial distribution of supraglacial debris is usually heterogeneous and depends primarily on the location of the entrainment zone and the transport of the sediment away from it (Bolch, 2011). The resulting debris cover thickness distribution hence is a function of the debris origin and deposition as well as the debris transport processes. Figure 2 schematically illustrates this connected system. Debris deposited on the accumulation zone is buried by snow and becomes entrained into the glacier. Debris can also be directly deposited onto the ablation zone, where the sediment usually remains on the glacier surface due to emergent glacier flow (Bolch, 2011). Furthermore, even subglacial debris can reach the glacier surface along shear horizons and become supraglacial debris (Hambrey et al., 2008).

1.1.2. Characteristics

Glacier dynamics and melt behaviours of debris-covered glaciers strongly differ from clean ice glaciers due to the insulating effect of supraglacial debris (Østrem, 1959; Nicholson and Benn, 2006), as displayed in Figure 3. Nakawo et al. (1986) have studied the debris thickness distribution on Khumbu Glacier in Nepal Himalaya and have observed an increase of the debris layer thickness in down-glacier direction. Across the glacier width, thin debris in the glacier centre was noted, with thicker debris away from the centre and then thinner debris again near
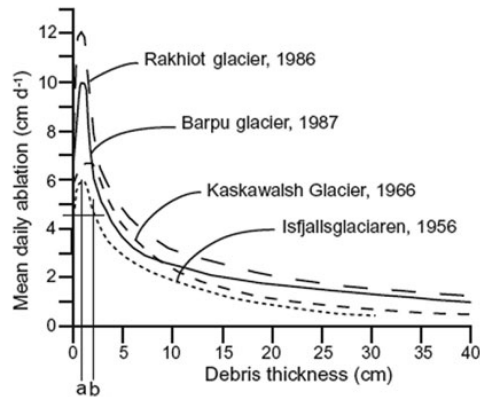
Figure 3. Relationship between supraglacial debris thickness and daily ice ablation rate on sample glaciers (Nicholson and Benn, 2006).

the glacier margin (Owen et al., 2003; Juen et al., 2014; McKinney, 2014; Bochiola et al., 2015; Schauwecker et al., 2015; Garg et al., 2017; Wang et al., 2017; Huang et al., 2018). The effects of a continuous debris cover in the ablation area of a glacier in a changing climate have been studied by Benn et al. (2012). According to the authors, reduced solid precipitation and increased melt result in decreased ice flux from the upper parts of the glacier. The influence of the debris cover on the ablation gradient leads to a reduction of the surface gradient, and the reduced driving stress in the lower ablation zone favours glacier slowdown and stagnation (Quincey et al., 2009). These processes are amplified by a positive feedback loop. This is the case for most debris-covered glaciers, independent of the effects of climate warming (Scherler et al., 2011; Konrad and Humphrey, 2000; Anderson and Anderson, 2016).

Anderson and Anderson (2016) summarise the effects of debris cover on glaciers as follows: A thick debris mantle from consistent debris input, independent of climate change, tends to reduce or reverse mass balance gradients, extend glaciers and reduce gradients of ice thickness and surface velocity under debris cover.

1.1.3. Challenges

The insulating effect of supraglacial debris on glacier ice is well studied and established. So far, however, remote sensing studies in the Hindukush-Karakoram-Himalaya region have failed to identify diminished rates of recession compared to clean ice glaciers (Kääb et al., 2012; Basnett et al., 2013; Gardelle et al., 2013) and have suggested an anomalous behaviour of debris-covered glaciers. An explanation for high ablation rates at the glacier scale has been attributed to the occurrence of ice cliffs and supraglacial lakes on debris-covered glaciers (Gardelle et al., 2012; Pellicciotti et al., 2015; Ragettli et al., 2016). This is in contrast to the low ablation rates under continuous debris covers due to inhibited melt and emphasises the importance of research on debris-covered glaciers.

Although melt under a homogeneous debris mantle is relatively well known and can be simulated with some confidence at the point-scale (Bozhinskiy et al., 1986; Mattson and Gardner, 1989, 1993; Nakawo and Rana, 1999; Nicholson and Benn, 2006; Hagg et al., 2008; Reid and Brock, 2010; Anderson and Anderson, 2016), all other aspects of debris influence on mass balance are

relatively poorly understood. Studies on distributed debris thickness estimates (Zhang et al., 2011; Foster et al., 2012; Rounce et al., 2015; Schauwecker et al., 2015), debris cover formation and supply (Kirkbride and Deline, 2013) and the dynamics of debris-covered glaciers (Rowan et al., 2015) are still very limited and affected by large uncertainties. A better understanding of the current and future state of debris-covered glaciers, in particular their surface characteristics, is crucial for estimating water resources and ice contribution to the oceans. In fact, Buri (2017) states that all studies that predicted global glacier mass balances and hence make estimates about the glacial contribution to sea level rise so far (Raper and Braithwaite, 2006; Kaser et al., 2006; Meier et al., 2007; Radić and Hock, 2011; Marzeion et al., 2012; Gardner et al., 2013; Marzeion et al., 2014; Huss and Hock, 2015) neglect debris cover. Also, a large part of the research interest in debris-covered glaciers is because their retreat dynamics endanger populations downstream (Quincey et al., 2005). Retreats of debris-covered valley glaciers have resulted in the formation of calving ice cliffs in moraine-dammed lakes in recent decades, leading to fatal incidents of glacial lake outburst floods, best known as GLOFs (Kirkbride, 2011).

Since supraglacial debris thickness is very heterogeneous and spatially dependent (Bolch, 2011), homogeneous debris cover models fail to accurately predict the dynamic glacier behaviour. Brock et al. (2010) emphasise that improved knowledge of spatial patterns of debris thickness distribution is required to develop distributed physically-based models for debris-covered glaciers. Furthermore, Carenzo et al. (2016) state that a large amount of input data of varying debris thickness is crucial for glacier melt modelling. The authors argue that the effect of debris cover on glacier-scale ice melt is usually assessed by integrating a single melt-reduction factor into the melt models. Reducing the process of melting in debris-covered glaciers to a single melt-reduction factor fails to adequately capture and model the extremely complex interactions within melting processes and thus produces oversimplified and potentially inaccurate results.

1.2. Hot Spot Himalayas

Debris-covered glacier tongues are widespread around the world in particular in mountain ranges with substantial debris production due to high relief and/or high erosion rates, such as the Himalayas and Karakoram. Debris-covered glaciers in this region show accumulation-area ratios (AARs) of 0.25–0.50 instead of the typical ratio of 0.60 for uncovered valley glaciers (Kirkbride, 2011; Scherler et al., 2011). Scherler et al. (2011) state that debris-covered glaciers are most common in the rugged central Himalayas, as shown in Figure 4. The authors investigated frontal variations of 255 Himalayan glaciers from 2000–2008 and detected no uniform response to climate change. Debris-covered glaciers showed little snout variations within the investigated period. The authors estimate the relative area of debris-covered glaciers to 18.3 % of the total glacier area and highlighted the importance of debris-covered glaciers to understand glacier retreat in this region. Different studies (e.g. Bolch et al., 2011, 2012; Benn et al., 2012; Kääb et al., 2012) show that Himalayan debris-covered glacier termini are not responding coherently to climate change despite a strong trend towards negative mass balance and surface lowering. Some Himalayan debris-covered glacier termini are advancing, others are stationary and yet others are retreating (Raper and Braithwaite, 2006; Scherler et al., 2011; Bolch et al., 2012). The discrepancy between debris-covered glacier mass balance and terminal response highlights the
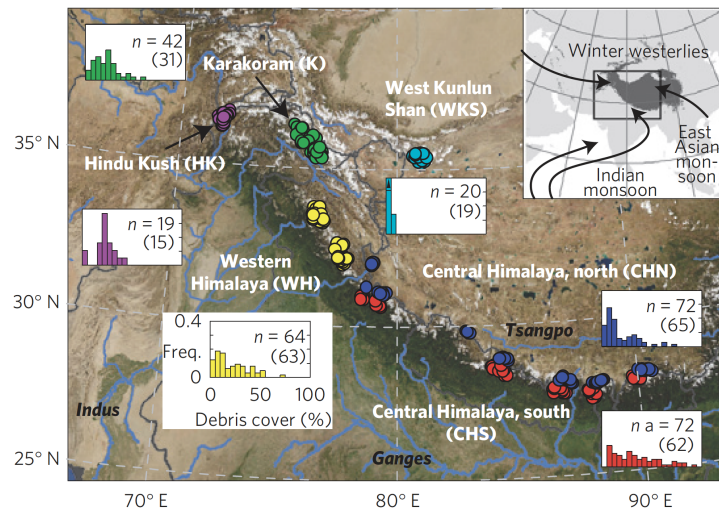
Figure 4. Regional distribution of debris-covered glaciers in the Himalayas analysed by Scherler et al. (2011). Location of glaciers (circles) grouped by region. The histograms give relative frequencies (y-axis, 0–40 %) of debris cover (x-axis, 0–100 % in 5 % bins). The number of studied glaciers is given in the upper-right corner of each histogram, measured frontal changes in parentheses. The inset globe depicts location of subset and atmospheric transport directions.

pressing need to understand the sometimes counter-intuitive effects of debris on glacier response. For this, debris cover must be understood integrally as a function of the debris entrainment zone and its transport away from it (Bolch, 2011).

1.3. Study Aim and Research Questions

This thesis aims to improve our understanding of the formation of supraglacial debris cover. To the best of my knowledge, it is the first study conducted so far which pursues a holistic approach for debris cover including numerous field measurements. This approach considers debris cover as the result of a connected system with 3 entities: (i) the location of the entrainment zone, (ii) the transport of the sediment away from it and (iii) the spatial distribution of debris on the glacier (Bolch, 2011). More specifically, this thesis intends to locate and estimate debris origin and supraglacial deposition as well as the transport of debris and to determine patterns of the supraglacial debris thickness distribution. The thesis is compiled as a case study of Zmuttgletscher, a glacier at the foot of Matterhorn in the western Swiss Alps. The proposed goals of this thesis will be addressed by the following research questions (RQs) and objectives, divided into the 3 entities mentioned above:

1.3.1. Debris Origin and Deposition

RQ1: «How are observed debris deposition zones linked to the contributing rock walls?»

Hambrey et al. (2008) state that one of the main debris sources for strongly debris-covered glaciers originate in the rock walls surrounding the glaciers. The main debris supply into the glacial system of Zmuttgletscher was found to be through snow and ice avalanches containing

eroded debris from the rock walls. I manually map the debris deposition cones on the slope toe of the headwall and link these to the respective contributing rock walls. I also compare the likewise manually mapped supraglacial debris deposition cones to deposition areas generated by a simple model for mass movement and deposition.

The total debris supply volume can be estimated by applying state of the art bedrock back-weathering rates for the Swiss alpine region (Matsuoka, 2008; Müller et al., 2014; de Haas et al., 2015) to the rock wall area. Furthermore, the debris concentration within the deposition cones is calculated to allow for a more detailed assessment of the connection between the actual debris input up-glacier and debris thicknesses down-glacier. For a separate part of the glacier, where accumulation solely happens by avalanching, the debris concentration within the glacier ice is estimated.

1.3.2. Debris Transport

RQ2: «What are the debris transport routes and how do they correspond with mapped debris deposition cones?»

The debris transport from the supraglacial deposition down-glacier happens within the glacier flow units (Kirkbride and Deline, 2013). For Zmuttgletscher, the flow units are visually assessed by considering the varying debris emergence locations, debris colour on the glacier tongue as well as glacier surface morphology. The flow units are compared to the ice flow velocity vector field for the lower ablation area (Mölg et al., in prep.). The flow unit boundaries should run parallel to the ice flow vectors.

1.3.3. Debris Thickness Distribution

RQ3: «How does the supraglacial debris thickness distribution vary spatially and how are potential patterns linked to the debris transport paths?»

The debris thickness distribution is determined by in-situ field measurements. The collected data is compared to observations and explanations for debris thickness distribution patterns proposed by state of the art literature. Combined with the ice flow velocity vector field, the annual debris flux is determined, which can be compared to the annual debris supply volume. Furthermore, the thickness measurements will be statistically assessed concerning their surface topography and spatial variability.

1.4. Thesis Structure

The short theoretical overview on debris-covered glaciers given in the introduction forms the thematic basis of this thesis. After that, Zmuttgletscher as the study area is introduced with a brief summary of its geography and glacial properties. The data chapter gives an overview of the image and terrain datasets as well as the field data that have been used for analysis in this thesis. In the methods section, the mapping, modelling and measuring techniques are described, and the results chapter then presents my research findings. An important part of

this thesis consists of the discussion chapter, where the three entities of debris are embedded in the scientific context and the research questions are readdressed in a synthesis. The thesis is wrapped up by concluding remarks and a quick outlook on potential future research concepts. The three chapters methods, results and discussion all follow the structure of the three entities, beginning with the debris origin and deposition, moving on to the debris transport and closing with the debris thickness distribution.

2. Study Area

Zmuttgletscher is a valley glacier in the western Swiss Alps close to Zermatt (Fig. 5). It has a projected surface area of approximately 16.5 km^2 and is surrounded by the three prominent peaks of Matterhorn (4478 m), Dent d'Hérens (4171 m) and Dent Blanche (4357 m). Its ablation area is heavily debris-covered, owed to the steep rock walls surrounding its accumulation basins with up to 1500 m of elevation difference and providing debris into the glacial system. The debris cover is composed of a large span of grain sizes, reaching between sand and big boulders (Fig. 6b). The ELA is at about 3100 m. This value is adopted from the mass balance measurements by WGMS (2017) on Findelengletscher, a valley glacier east from Zermatt and merely 13 km away from Zmuttgletscher 5c. The accumulation area of Zmuttgletscher consists of three tributary glaciers: Schönbielgletscher from the north, Stockjigletscher from the west and Tiefmattengletscher from the south; Zmuttgletscher mainly describes the ablation area. Today, Tiefmattengletscher is the main (if not the only) contributing glacier to Zmuttgletscher, and only this tributary is dynamically relevant for the debris-covered ablation zone. Therefore, the scope of this thesis is narrowed to Tiefmattengletscher as main accumulation basin for the ablation area of Zmuttgletscher. The two other tributaries will not be considered. Henceforth, when mentioning Zmuttgletscher, I mean the coherent system of Tiefmattengletscher as accumulation and Zmuttgletscher as ablation area (labelled as investigated glacier area in Fig. 5a).

The debris-covered glacier tongue at 2250 m has a very flat surface of 5.7° over the lowest kilometre and exhibits numerous ice cliffs cutting into the terrain. The ablation area is longitudinally traversed by two distinctive crests. The glacier tongue slightly deviates to the east and is embedded between two lateral moraines (Fig. 5a and 7). Further up-glacier, at an elevation of approx. 2700 m, the glacier flows over an edge in the bedrock topography. This results in an icefall with big crevasses across the entire glacier width. In the eastern part of the accumulation area, an additional icefall at 2850 m can be observed.

The different response of debris-covered glaciers to climate change compared to clean ice glaciers is well observable in this alpine area. Findelengletscher, a clean ice valley glacier, has climatic properties comparable to Zmuttgletscher, given the geographic proximity. However, Figure 8 illustrates the cumulative length changes of the two glaciers between 1892 and 2016. Zmuttgletscher lost ice mass quite linearly until 1980 and has experienced nearly stagnation since then. Contrary to this, Findelengletscher shows much more variations in its glacier length and lost more than 2500 m for the whole time span, while Zmuttgletscher only retreated by
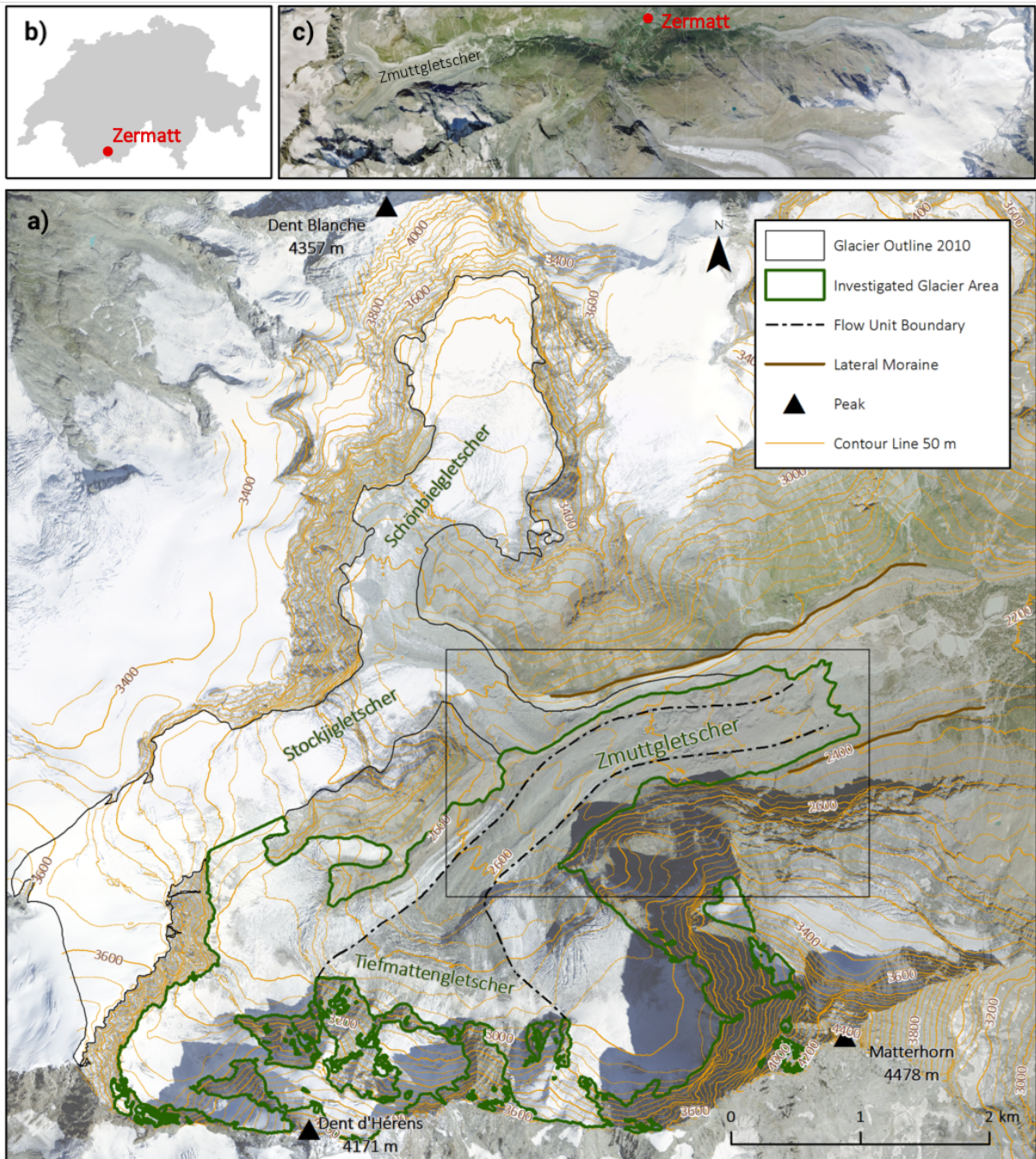
Figure 5. Overview maps of the study area. a). Outline of Zmuttgletscher composed of its three tributary glaciers. The green outline marks the investigated glacier area. The dashed-dotted lines mark the three major Flow Units 1 to 3, labelled with their respective number. Peaks and the lateral moraines are displayed as well. The box around the glacier tongue marks the frame of Figure 12. b) Inset map of the location of Zermatt. c) Zoom into the inset map to Zermatt, where the positions of Zmuttgletscher and Findelengletscher are labelled (swisstopo, 2018).

Figure 6. Impressions of the debris cover on Zmuttgletscher. a) Collapsing side walls at a deep measuring point. b) Large grain size variations of the sediment ranging between sand and big boulders (September 2017, pictures by N. Mölg).
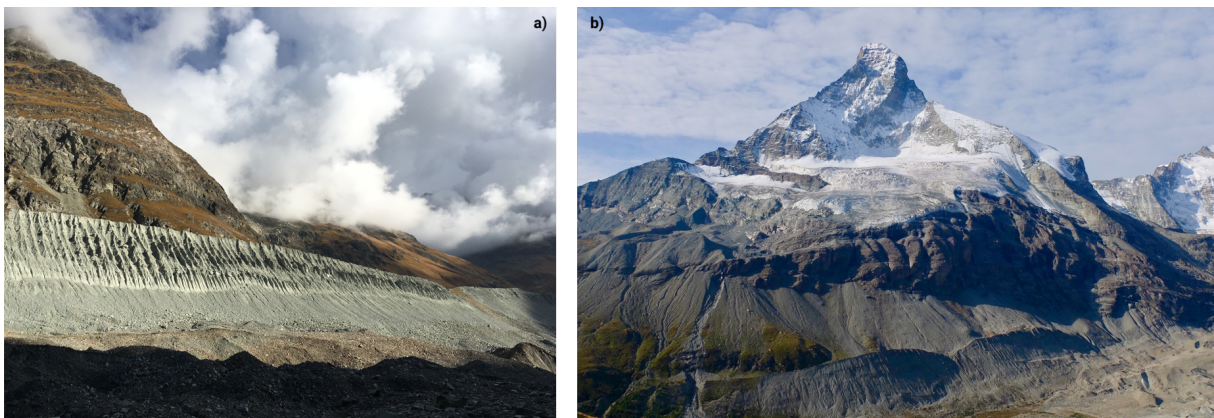
Figure 7. Lateral moraines of Zmuttgletscher. a) Left lateral moraine, b) right lateral moraine beneath north wall of Matterhorn (August and September 2017).
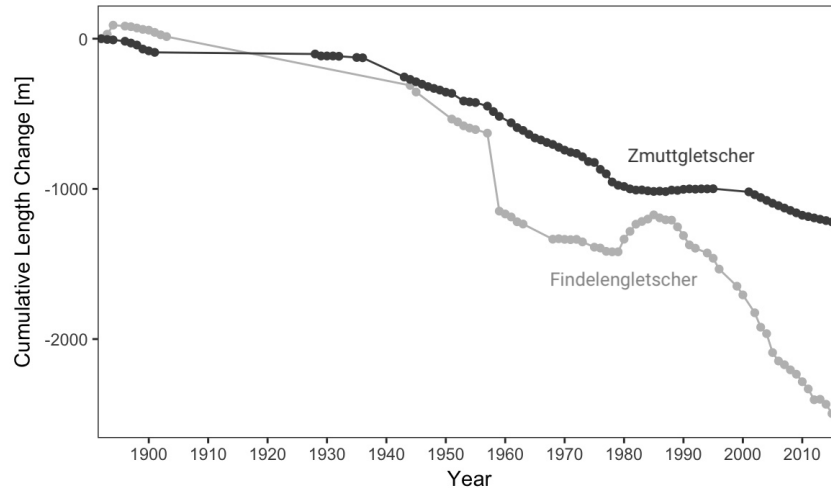
Figure 8. Cumulative length changes of Zmuttgletscher and Findelengletscher between 1892 and 2016. Data from GLAMOS (2018).

1200 m. This vast difference can be explained with the insulating effect of the debris cover. Zmuttgletscher is one of the largest debris-covered glaciers in the Alps, together with Unteraargletscher in the Bernese Oberland (Switzerland) and Miage Glacier in the Mont Blanc massif (France) (Deline, 2005). The glacier is quite easily accessible for fieldwork and has been explored since 1892, when the Swiss Glacier Monitoring Network started to measure the glacier's length changes. Even though my thesis does not take any temporal variations into account, it is a big advantage to conduct my research on a glacier whose length has been investigated for so long. This allows for possible future research projects to combine my findings with changes over time. Hence, Zmuttgletscher represents a good case study to investigate supraglacial debris cover.

2.1. Terminology

In this short section, I introduce some site-specific terms that I will use to describe the methods and results of my analyses. These terms will allow me to characterise certain features more easily and detailed at the same time.

During my work on this project, it became clear that there are three rather distinctive units to Zmuttgletscher. This is owed to the topography of the glacier's accumulation area. This accumulation area is composed of three parts. There are two big basins underneath Dent d'Hérens and Matterhorn respectively, where the glacier ice is covered by perennial snow and no debris is yet visible on the ice surface. This is owed to the bergschrund (at approximately 3200 m) lying above the ELA. In between these two basins, the bergschrund lies a little deeper (at approximately 2900 m) and hence beneath the ELA. This marks the middle part of the three accumulation parts to Zmuttgletscher. The glacier ice here is debris-covered all the way up to the headwall and avalanche deposition cones. This implies that accumulation for this glacier part solely happens by avalanching onto the glacier area which is already part of the ablation area. This area is particularly interesting for my thesis, as debris deposited in this glacier area stays on the glacier surface and is not entrained in the glacier ice. Therefore, I do not only focus on the whole glacier for my research, but I also perform analyses only for this part of the glacier.

This heterogeneous topography suggests that the whole glacial system of Zmuttgletscher should be categorised into these three units to accurately discuss the results in this thesis. For this purpose, I make use of the terms *Flow Unit 1*, *Flow Unit 2* and *Flow Unit 3* for the glacier area of these respective units. The three flow units are further subdivided into subcategories, which I refer to by *Flow Unit 1a*, *Flow Unit 1b* etc. To address the headwall above Zmuttgletscher, I use the phrases *Headwall 1*, *Headwall 2* and *Headwall 3*, which correspond to the flow unit divisions. Figure 5a illustrates this division of Zmuttgletscher. For certain results, I already presume this division and present my findings partitioned into these units.

The headwall above Zmuttgletscher consists of hanging glaciers, patches of perennial snow and bare rock wall. Please note that the phrase *rock wall* refers to these bare bedrock areas, while the term *headwall* describes the whole wall face including the rock walls as well as the snow and ice bodies.

Many features of the debris cover discussed here are related to its surface aspect. By aspect, I do not mean it in the conventional sense of the four cardinal points, but rather in relation to the glacier ice flow direction. Therefore, when I speak of *left* and *right*, I always mean relative to the ice flow. On the glacier tongue, left almost perfectly points to the north, while right points to the south.

2. Study Area

3. Data

3.1. Provided Data

To answer my research questions, I use a variety of data ranging from field data which I acquired through intensive fieldwork through orthorectified aerial photograph archives to modern digital terrain models. I received a dataset consisting of 13 orthorectified images (orthophotographs) which where created from aerial photographs of the study region between 1946 and 2017 (Tab. 1). The aerial photographs were digitised and orthorectified by swisstopo (2018) and are provided in the Swiss coordinate system LV03 (SRID: 21781). The UAV photographs were orthorectified by Mölg et al. (in prep.). Having data spanning a considerable time period allows the detection of sporadic and more importantly periodic events, such as the evolution of the avalanche deposition cones. This is paramount in understanding glacial processes, in particular debris deposition. The temporal variations are only considered for the deposition cone mapping (see section 4.1.2).

Seeing that glacial debris deposition and transport processes are inherently 3-D processes, elevation data is an integral fundamental dataset for my analyses. I use a digital terrain model (DTM) as an underlying dataset. The swissALTI3D product, created and maintained by swisstopo (2018), is a suitable dataset to investigate my research questions. I chose the latest available dataset which covers all of the study region, i.e. the DTM from 2010, which is also provided in the coordinate system LV03. The DTM provides 3-D elevation data of the whole study region in a spatial resolution of 2 m and does not include structures or vegetation.

In addition to the DTM of 2010, I received the high resolution orthorectified aerial image product SWISSIMAGE from 2010 (swisstopo, 2018). The image has a spatial resolution of 25 cm and covers the whole study area. Again, this dataset is also made available in the coordinate system LV03. To be able to compare the SWISSIMAGE dataset with a digital terrain model, both datasets should show similar data acquisition periods. Thus, I incorporate the SWISSIMAGE of 2010 as main reference in my steady state analyses, i.e. where I do not consider temporal variations.

To calculate flow velocities and debris fluxes on the glacier tongue, I received flow velocity point measurement data acquired between 2016 and 2017 by Mölg et al. (in prep.) (Fig. B.1). Their velocity data are obtained from two orthophotographs with a spatial resolution of 0.5 m, derived from an unmanned aerial vehicle. The data cover the range from the glacier terminus up until my highest field measurements.

Table 1. Provided orthophotograph dataset by swisstopo (2018) and Mölg et al. (in prep.). The orthophotograph from 2016 only covers the glacier tongue of Zmuttgletscher.

Year	Spatial Resolution [m]	Source	Use	Comment
1946	0.5	swisstopo	Yes	Mapping of the deposition cones
1961	0.5	swisstopo	No	Insufficient quality
1977	0.4	swisstopo	Yes	Mapping of the deposition cones
1983	0.15	swisstopo	No	Spatial coverage too small
1988	0.35	swisstopo	Yes	Mapping of the deposition cones
1995	0.15	swisstopo	No	Insufficient weather conditions
2001	0.35	swisstopo	Yes	Mapping of the deposition cones
2005	0.5	swisstopo	Yes	Mapping of the deposition cones
2007	1.0	swisstopo	Yes	Mapping of the deposition cones
2010	0.25	swisstopo	Yes	Mapping of the headwall, flow units, deposition cones
2013	0.25	swisstopo	Yes	Mapping of the deposition cones
2016	0.25	Mölg et al.	Yes	Mapping of the flow units

3.2. Field Data

To complement the readily available datasets and to have high quality in-situ measurements, I actively collected debris cover thickness data. This data was acquired in fieldwork between 26th and 28th September 2017. I collected georeferenced in-situ debris thickness measurements on the glacier tongue of Zmuttgletscher. I acquired thickness measurements in three glacier cross-section transects and one smaller-scale transect covering a ridge–trough slope. Along with the location and thickness of the in-situ debris thickness measurement points, I also collected meta data on the daily conditions and documented the locations and interesting features with photographs.

I imported the data into a geographic information system (GIS) to be able to analyse the data in regards to my research questions. The spatial analyses are performed in ArcGIS, while the statistical analysis and data visualisations are made in RStudio.

4. Methods

4.1. Debris Origin and Deposition

This section covers the source of the supraglacial debris on Zmuttgletscher. To quantify this origin, I only consider the rock walls surrounding the accumulation area of the glacier. Bolch (2011), Hambrey et al. (2008) and Nakawo et al. (1986) state that supraglacial debris deposition can originate in subglacial bedrock erosion and then be transported to the ice surface via shear horizons, thrusting or folding. The relative amount of supraglacial debris with such a subglacial origin is, however, very small (Hambrey et al., 2008) and thereby deemed negligible for the scope of my thesis.

4.1.1. Rock Walls

To map the rock walls above Zmuttgletscher, I work with the SWISSIMAGE from 2010. I primarily map the glacier area of Zmuttgletscher including hanging glaciers and areas of perennial snow in the headwall. The remaining area above Zmuttgletscher and underneath the ridge of the glacial catchment area (calculated from the DTM) is classified as rock wall area. Since the generated shape files represent only the projected 2-D area, the mapped rock wall area are converted into a 3-D feature using the DTM as 3-D surface input.

4.1.2. Deposition Cones

The debris input for Zmuttgletscher happens via constant erosion of the rock wall areas. This is suggested by consultation of the aerial images between 1946 and 2010 for the headwall of Zmuttgletscher: No single rockfall event is visible for this whole time period. Hence, I only consider constant rock wall erosion as debris input.

The eroded material is entered into the glacial system through snow and ice avalanches onto the glacier. The aerial images between 1946 and 2010 suggest that avalanche events in the study area are persistent in their location over time – in other words, avalanches seem to occur in similar places over the years where data is available. Mentioned avalanches thus reproduce their deposition cones year after year. I visually map the average range of these deposition cones to be able to compare the deposition range with the results from the MTD model output (see section 4.1.5).
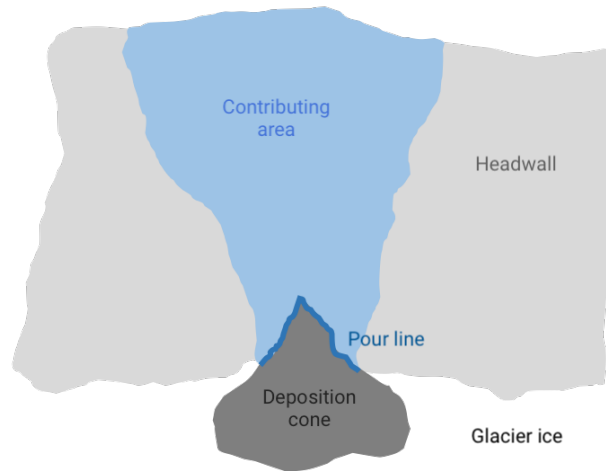
Figure 9. Schematic explanation of the computation of the contributing area per deposition cone. This front view on the headwall shows that the contributing area is calculated for the entire contact line (pour line) between the deposition cone and the headwall.

4.1.3. Contributing Area

In order to quantify the amount of debris per deposition cone, the catchment area of each mapped cone is calculated in ArcMap. For each cone, I draw a so-called pour line along the contact line between the cone and the headwall. Via the computed flow direction grid derived from the DTM, the catchment areas for each of these pour lines are determined (Fig. 9). The actual contributing rock wall area per deposition cone is calculated by converting the catchments into 3-D features and intersecting them with the mapped rock walls.

4.1.4. Erosion Rates

For the constant erosion assumed for the rock wall areas of Zmuttgletscher in the southern Swiss Alps, a range of 0.1 mm/a (Matsuoka, 2008) to 1 mm/a (Müller et al., 2014) are reasonable. Since long-term rates are generally higher than 1 mm/a (de Haas et al., 2015), I work with rock wall retreat rates of 0.1 mm/a as a minimum and 2 mm/a as a maximum value in this thesis.

4.1.5. Mass Transport and Deposition Model

The most time-consuming mapping work that is carried out in the scope of this thesis is the digitising of the deposition cones. I am able to consult multiple orthophotographs acquired over a period of almost 70 years. The mapped cones are thus arguably a well suited proxy of the actual avalanche deposition areas. The major drawback of manually interpreting and mapping orthophotographs is the time consuming nature of the task in combination with the high subjectivity of interpretation and thus high potential for biases according to the interpreting person.

To address mentioned issues of the time intensive nature of the task and potential interpretation bias, I make use of a simple Mass Transport and Deposition model (MTD) developed by Gruber (2007), and apply it to the study site of Zmuttgletscher. The aim is to evaluate the automatic reproduction of avalanche deposition cones and to qualitatively assess the model performance.

The MTD is a fast and mass-conserving algorithm to parametrise mass transport and deposition and does not include effects of kinetic energy. Therefore, it neglects potential uphill flow. These limitations do not influence my analyses, as I am interested in the supraglacial avalanche deposition and hence do not require uphill modelling. The simple algorithm is very fast, and the model can therefore be calculated over large areas. To evaluate the algorithms efficiency, Gruber (2007) as well as Böckli (2008) successfully applied the algorithm to situations with multiple small and frequent snow avalanches in steep terrain. This arguably shows that the MTD algorithm is well suited for my research questions and is thus transferable to the settings of Zmuttgletscher.

The model requires the following raster datasets:

- Flow direction per cell (derived from DTM),

- Initial mass I per cell (release area),

- Maximum deposition D_{max} per cell.

When the model is run, the initial or input mass I is released and flows downhill along the steepest slope. The flow direction follows a *multiple-neighbour flow* algorithm, meaning that the flow process can take place not only in one but in several neighbouring cells. This allows for modelling a diverging flow behaviour, which is well suited for my desired application.

The flowing mass M is transported downstream according to a flow direction algorithm. Each cell receives a fraction of the mass cd_{NB} from its neighbour cell. The deposition D in a cell is limited by the local deposition maximum D_{max} and by the availability of the flowing mass M. D_{max} is independent of mass flow and is determined by local characteristics, e.g. as a function of the slope of the terrain.

$$D = \begin{cases} M & \text{if } M < D_{max} \\ D_{max} & \text{if } M \geq D_{max} \end{cases}$$

The mass flow F_{NB} into each neighbouring cell is given by the remaining mass after deposition $(M - D)$ multiplied by the mass division fraction cd_{NB}.

$$F_{NB} = (M - D) \cdot cd_{NB}$$

Only local characteristics determine the maximum deposition D_{max}. A simple function is used to relate D_{max} to the local slope angle β that is assumed to be its most important determinant:

$$D_{max} = \begin{cases} (1 - \frac{\beta}{\beta_{lim}}) \cdot D_{lim} & \text{if } \beta < \beta_{lim} \\ 0 & \text{if } \beta \geq \beta_{lim}. \end{cases}$$

D_{lim} is the limiting deposition, i.e. the maximum deposition that would occur on horizontal terrain. The limiting slope β_{lim} denotes the maximum terrain steepness at which some mass is deposited. D_{lim} and β_{lim} are the two parameters that need to be entered into the model.

I conduct a sensitivity analysis for the two model parameters D_{lim} and β_{lim} in the case study of Zmuttgletscher. The model is run in RStudio. I resample the DTM from a 2 m spatial

resolution to 10 m, since this resolution produces the most accurate deposition areas for small avalanches (Böckli, 2008). I run several initial mass scenarios to identify ideal input mass values for headwall areas containing big hanging glaciers. The calving at large hanging glacier fronts regularly produces large avalanche deposition cones, which are not met with a constant input mass for the whole headwall area. To avoid this problem, higher input values for raster cells covering such hanging glacier fronts are chosen. The spatial distribution of the input mass is dispayed in Figure C.2.

4.1.6. Debris Supply

As I collect debris thickness measurements on the glacier tongue (see section 4.3.1), it is possible to combine these measurements with the ice flow velocities (see section 4.2.2) to assess a debris flux in the ablation area (see section 4.3.3). Assuming that the amount of debris being transported through a cross section of the glacier equals the amount of debris entered into the system, the supraglacial debris flux can be compared to a calculated debris supply. They most likely will not be of the same size, as there is still debris embedded in the glacier ice and thus my calculated debris flux only describes the supraglacial share. Nevertheless, it is still interesting to compare the orders of magnitude for the two quantities. Furthermore, it will allow an assessment of the two erosion rate input scenarios.

To quantify the debris supply to the glacial system from the rock walls, the actual rock wall area is multiplied by the erosion rate assumed for the study site. As I am working with a range for the erosion rates, two scenarios are considered: One with the minimum erosion rate (0.1 mm/a) and one with the maximum erosion rate (2 mm/a). This results in two scenarios of total amount for the debris input to Zmuttgletscher.

In a next step, the debris supply is partitioned according to the deposition cones. The individual contributing rock wall areas per deposition cone are multiplied with the two erosion rates, yielding the debris input per deposition cone.

Debris Concentration

Analogously to the MTD model, where a constant input of 1 m of snow is implemented for the whole headwall (see section 5.1.3), the absolute amount of debris per deposition cone can be converted into a relative debris concentration when the amount of snow is also taken into account:

$$C_{snow} = \frac{E \cdot A_{rock}}{H_M \cdot A_{cont}}$$

The debris concentration in the snow deposition C_{snow} is calculated by dividing the actual debris amount (the erosion rate E multiplied by the contributing rock wall area A_{rock}) by the volume of snow (the height of the flowing mass H_M multiplied by the total contributing area A_{cont}). However, to derive the actual debris concentration within the cones, I cannot calculate with 1 m of snow, since the snow is compacted when it is deposited in the form of avalanches. SLF (2017) suggests a density for fresh snow ρ_{snow} of 100 kg/m^3 and a density for avalanche-deposited snow within the deposition cones ρ_{aval} of 300 kg/m^3. The increased density within the deposition

cones means that I have to calculate the debris concentration with a smaller snow column than $1\ m$. The compression factor which takes this into account is the ratio of the two densities. For the debris concentration within the avalanche-fed deposition cones C_{aval}, this changes the equation as follows:

$$C_{aval} = \frac{E \cdot A_{rock}}{H_M \cdot A_{cont}} \cdot \frac{\rho_{aval}}{\rho_{snow}}$$

With time, the deposition cones are compressed to glacier ice by processes of firnification and metamorphosis. This again alters the concentration of debris. To calculate the debris concentration in glacier ice, I hence have to proceed analogously. Here, the compression factor for the metamorphosis from fresh snow to ice has to be considered. The density for ice ρ_{ice} is 917 kg/m^3 (Cuffey and Paterson, 2010), which gives the following equation for the debris concentration within glacier ice C_{ice}:

$$C_{ice} = \frac{E \cdot A_{rock}}{H_M \cdot A_{cont}} \cdot \frac{\rho_{ice}}{\rho_{snow}}$$

I calculate the englacial debris concentration C_{ice} only for Flow Unit 2. In this unit, accumulation happens solely by avalanches which generate the debris supply at the same time. The other two flow units presumably also experience conventional accumulation by precipitation. This changes the englacial debris concentration. An approximation with this formula would not be accurate for the glacial cross-section but only for distinctive debris septa within the ice.

4.2. Debris Transport

4.2.1. Flow Units

The flow structure of a glacier determines the englacial pathways of debris (Hambrey et al., 2008). I intend to asses these flow paths as shown by the example of Jennings et al. (2014), who divided Vadrec del Forno glacier into its flow units (Fig. 10). This allowed the authors to assess the debris transport routes.

The flow structure of Zmuttgletscher is manually mapped in ArcGIS using the SWISSIMAGE 2010. The distinction of the three major Flow Units 1, 2 and 3 is based on the debris emergence location out of the ice onto the glacier surface. The subdivision of the three major flow units into finer subunits is achieved by taking the debris emergence location as well as the different rock colours for the debris-covered part of the glacier into account (Fig. 11). The resulting subunits are compared to the glacier surface topography. Since glaciers with multiple accumulations basins tend to form ice stream interaction medial moraines (Anderson, 2000; Gibson et al., 2017), the two distinctive crests described in chapter 2 should have a subunit boundary running all along their ridge.

The three major flow units divide the glacier area of Zmuttgletscher into three sections (see section 5.2.1). This division allows the debris thickness measurements on the lower glacier tongue to be associated with the deposition cones in the accumulation area of the glacier.
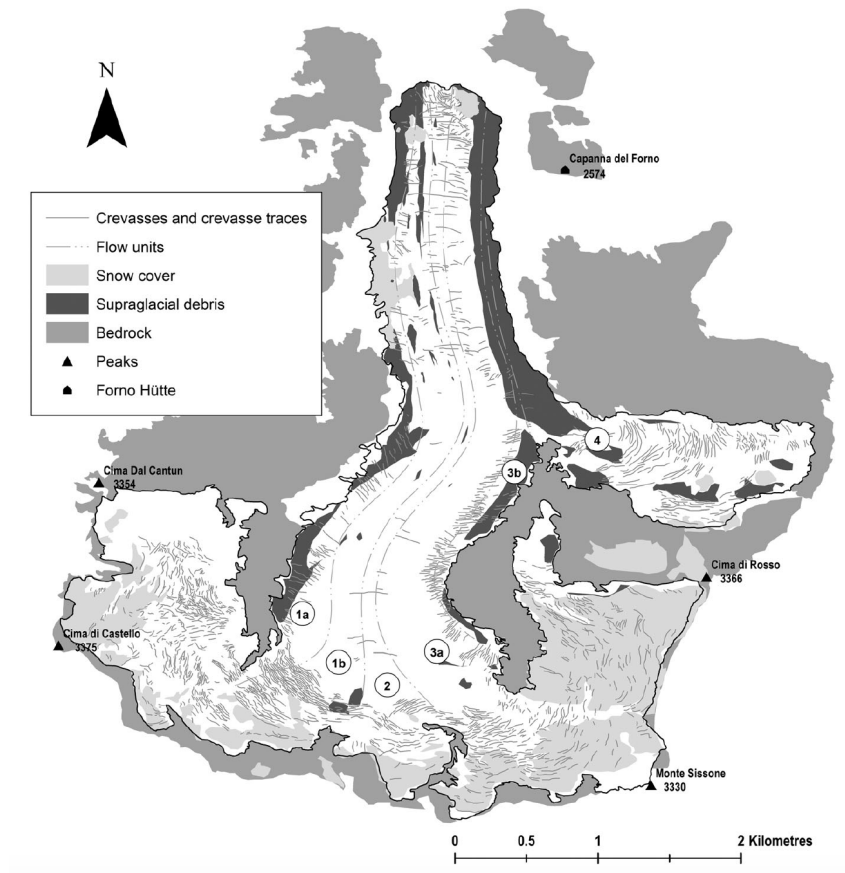
Figure 10. Flow units of Vadrec del Forno glacier, Switzerland (Jennings et al., 2014). The flow units are indicated with circled numbers and separated by dashed-dotted grey lines.

Figure 11. Colourful supraglacial debris bands on the ablation area of Zmuttgletscher (September 2017).
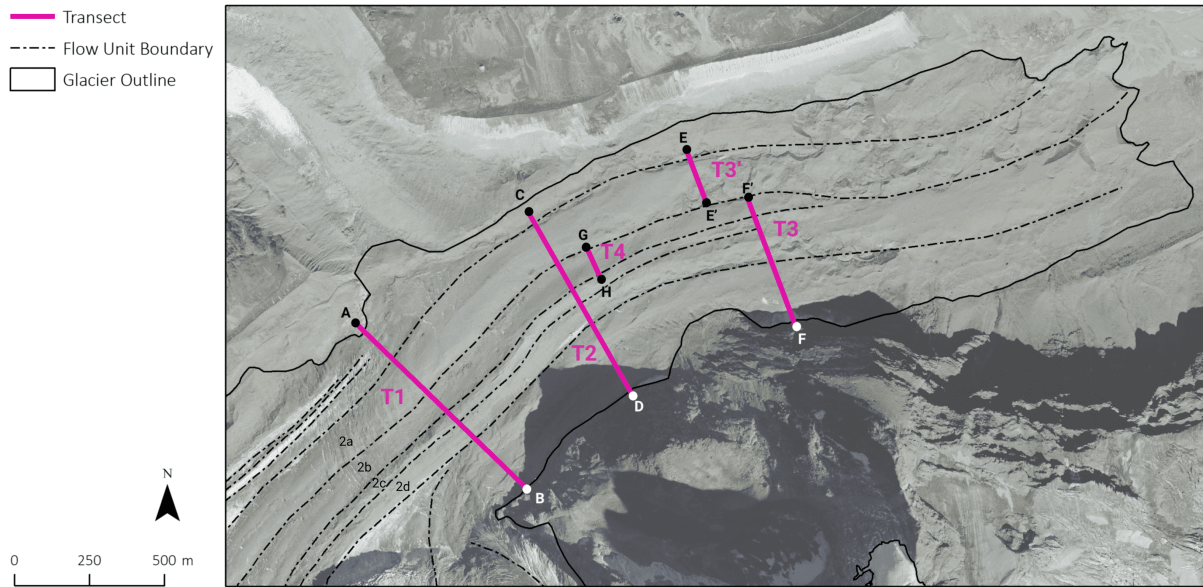
Figure 12. Location of the debris thickness measurement transects. The pink labels indicate the transect number, the bold letters mark the start and end points of the transects. In the lower left corner, the flow subunits are given. Transect 3 had to be interrupted and resumed due to a big ice cliff.

4.2.2. Flow Velocity

The flow velocities used to verify the flow units and to calculate the debris flux (see section 4.3.3) are provided by Mölg et al. (in prep.) (Fig. B.1). I interpolate the point measurements in ArcGIS by applying universal kriging. Kriging has been identified as having similar or above average accuracy when compared to other spatial interpolation methods. This is largely due to kriging using more advanced weighting techniques (e.g. semi-variogram method) to calculate new values from given data points, albeit being computationally more expensive (see Setianto and Triandini, 2013; Li and Heap, 2014). I interpolate my data using universal kriging, as computation power does not pose an issue seeing the relatively small number of data points.

4.3. Debris Thickness Distribution

4.3.1. Field Data

During my fieldwork, we took a number of debris thickness measurements on the tongue of Zmuttgletscher. In a first step, we took thickness measurements at three cross-sections of the terminus (Transects 1 through 3). We then took an additional fourth profile across a ridge-trough slope with the slope facing left (Transect 4). The location of the transects on the glacier tongue is displayed in Figure 12. We took our measurements by digging holes into the debris cover with a pickaxe and a shovel. With the pickaxe put horizontally over the holes to slightly level out the measurement, we measured the debris thickness with a folding rule (Fig. 13a). The measuring points in Transects 1 through 3 represent the average thickness of three measurements arranged in an equilateral triangle with $1\ m$ side lengths (Fig. 13b). When a measurement showed a thickness of more than $20\ cm$, a single measurement was used for one measuring point

4. Methods

Figure 13. Setup for the debris thickness measurements. a) Horizontally placed pickaxe and folding meter. The debris thickness is measured at the lower level of the pickaxe shaft. b) Three debris thickness measurements (red dots) with a respective distance of 1 m to each other were taken and averaged to compose one single measuring point of debris thickness.

instead of an average. The reasoning behind this is that Figure 3 shows no notable decrease in ablation from debris 20 cm or thicker. I thus argue that the variability of thicknesses of more than 20 cm is not crucial in regards to my research questions. This also led to us not digging deeper than 60 cm due to questionable debris integrity and the potential danger of collapsing side walls (Fig. 6a).

The centroids of the equilateral triangles used as measurement points along the cross-section transects (1 through 3) are spaced roughly equally every 30 m. Distances vary according to GPS accuracy and accessibility. It was important to have finer grained information in areas of particular interest (i.e. interesting formations, such as crests). We therefore sometimes deviated from the defined 30 m distance between thickness measurements. For instance, on a pronounced ridge, we took thickness measurements on the ridge itself as well as on the left and right slope just underneath the ridge to assess the small-scale thickness variability.

For Transect 4, a slope facing left was selected beneath a prominent crest. During the recording of the Transects 1 to 3, we noticed that the thickness of debris on the left slopes tended to be thinner than on the right ones. We decided to investigate a left-facing slope because it again seemed to be more feasible: The intention of this slope-profile was to determine the small-scale gradual course of the debris cover and to observe gravitational redistribution processes. This gradient should be visible on both the left and right side of the crest, while on the left simply being less pronounced.

Table 2. Characteristics of the four debris thickness measurement transects on the glacier tongue of Zmuttgletscher.

	Width [m]	Average Elevation [m]	Number of Points	Spacing between Points [m]
Transect 1	665	2538	23	30
Transect 2	506	2489	24	30
Transect 3	418	2495	20	30
Transect 4	109	2574	54	2

The characteristics of the four transects are compiled in Table 2. The following questions should be answered with the measurements of the transects:

(i) **Gradation:** What does the change of thickness of the debris cover look like in direction of ice flow, i.e. towards the glacier tongue?

(ii) **Topography:** How do the topographic features of slope, aspect and topography classes correlate with the debris thickness distribution?

(iii) **Variability:** How does the small-scale debris thickness variability (i.e. the relative standard deviation) correlate with the actual debris thickness?

(iv) **Slope profile:** Which processes underlie the debris thickness progression of the high-resolution slope-profile (Transect 4)?

To answer the posed questions meaningfully and significantly, some form of classification becomes necessary. I thus used my field notes and the DTM to manually divide the collected debris thickness measurements into two categories for the aspect («left» and «right») and three categories for the topography («ridge», «slope» and «trough»). Furthermore, I calculated the slope raster from the DTM in ArcGIS to investigate the relation between debris cover and surface slope.

4.3.2. Statistical Methods

Statistical analyses offer great insight into the underlying characteristics of datasets. The collected fieldwork data is statistically analysed in RStudio. The individual methods are explained in more detail in the following sections. A statistical significance level of $\alpha = 0.05$ is chosen for all performed tests in this thesis. The null-hypothesis ($\mathcal{H}_0$) of the individual research questions is rejected if the corresponding p-value is lower than α.

Kruskal-Wallis Test

The Kruskal-Wallis test is a non-parametric test for the equality of means for more than two independent samples which contain interval-scaled, not normally distributed data (Rogerson, 2015; UZH, 2018). The test-specific $\mathcal{H}_0$ for the Kruskal-Wallis test is: «The mean ranks of the samples are equal.» The requirements are met for the mean value comparison tests for (i) the

gradation of the debris thickness and (ii) the correlation of the surface topography classes with the debris thickness. The correlation analysis for the topography classes is conducted for the thickness measurements of all three transects combined. Seperate analyses for each transect are not possible, as the sample size for the «trough» sample is too small (only two for Transects 1 and 3).

Mann-Whitney Test

The Mann-Whitney test is a non-parametric test for the equality of means for exactly two independent samples which contain interval-scaled, not normally distributed data (Rogerson, 2015; UZH, 2018). The test-specific $\mathcal{H}_0$ for the Mann-Whitney test is: «The rank sums of the samples are equal.» The requirements are met for the mean value comparison tests for (ii) the correlation of the aspect with the debris thickness. I conduct a correlation analysis for the thickness measurements of all three transects combined as well as three individual analyses for each transect.

One-Way ANOVA

The single factor analysis of variance (One-Way ANOVA) analyses the equality of means for more than two independent samples which contain interval-scaled, normally distributed data with equal population variances, i.e. homoscedasticity (Rogerson, 2015; UZH, 2018). The requirements are met for the mean value comparison tests for (ii) the correlation of the slope with the debris thickness and (iii) the correlation of the debris thickness with the the variability. The assessment of the regression analyses is based on the coefficient of determination R^2.

For the surface slope, I conduct two different regression analyses: one with the slope value of the single pixels where the actual measurements are taken, and one where I average the slope over a buffer of 3 m radius around the measuring points.

For the variability, I perform a regression analysis where I try to predict the debris thickness with the relative standard deviation. For this, I exclude all measuring points where only one measurement was taken. For the remaining points, I divide the standard deviation by the mean debris thickness to receive the relative standard deviation. This step ensures that I avoid autocorrelation where the larger standard deviations are put in relation to their presumably larger debris thicknesses.

4.3.3. Debris Flux

To compare the amount of debris lying on the glacier tongue with the input into the system (see section 4.1.6), the debris flux for the three cross-section transects can be calculated. The debris thickness measurements are integrated to a 2-D surface by taking the distance between the measuring points into account. This yields a debris integral D_{int} in m^2, which can be combined with the flow velocities V in m/a to the actual debris flux Q as a volume in m^3/a:

$$Q = D_{int} \cdot V$$

Since we do not have any thickness measurements in Transects 2 and 3 for Flow Unit 1 and only

a limited number of them for Flow Unit 3, a detached analysis of the debris flux only for Flow Unit 2 is also performed.

4.3.4. Debris Emergence Rate

With the debris integrals for Transects 1 through 3 and the respective distances between the transects, it is possible to calculate a debris emergence rate between Transect 1 and 2 as well as between Transect 2 and 3. The distance d divided by the integral difference ΔD_{int} yields the distance required for the emergence of debris. Further multiplying this required distance with the average width of the two transects w results in the debris emergence rate ER in m/m.

$$ER = w \cdot \frac{d}{\Delta D_{int}}$$

4.4. Uncertainties

For the visual mapping of the rock wall areas above Zmuttgletscher, the classification of the headwall into rock walls or perennial snow/hanging glacier area was carried out subjectively on the basis of a single orthophotograph. Patches classified as perennial snow could simply be still covered by seasonal snow. However, these uncertain snow areas are mostly very small and would not produce a large error for the estimation of debris input, especially considering the small erosion rates that are applied to the rock wall areas. Another challenge is to make sure that the upper limits (ridges) of the calculated contributing areas match the manually mapped limits of the headwall classification. Where necessary, the contributing area limits are adjusted manually to ensure consistency.

The calculation of the debris input volume is based on literature values for backweathering rates assumed to be accurate for the geographic region of Zmuttgletscher. It spans a rather large range between 0.1 and 2 mm/a, where the maximum exceeds the minimum by 2'000 %. However, since bedrock erosion is highly dependent on the lithology (Bolch, 2011) as well as surface slope and curvature (Heimsath and McGlynn, 2008), which I do not consider in this thesis, it makes sense to apply a wide range of scenarios. After all, the comparison of the debris input volume with the debris flux may allow to narrow the erosion rate range in the discussion part.

The attempt to reproduce the deposition cones by the MTD algorithm is based on a sensitivity analysis with a constant input mass for the whole headwall area, except for the calving fronts of the four big hanging glaciers (Fig. C.2). This most likely does not meet real conditions, as snow deposition is highly dependent on wind conditions and the surface slope (Gruber, 2007). This implies that the results for the MTD model run must be taken with caution. Furthermore, the simulation is run with a DTM that already includes the deposition cones and hence models the deposition onto those cones, which is prone to produce a larger spatial dispersion.

The distinction of the flow units is highly uncertain where the glacier is not debris-covered or even covered by snow on the orthophotograph. This can greatly influence the connection of the deposition cones and their contributing rock wall area with the down-glacier thickness measurements. To minimise this uncertainty as much as possible, the flow units are verified with the ice flow vector field. However, this is only available for the lower part of the glacier

tongue. The ice flow vector field itself is assumed to have low uncertainties. It was filtered using a visually defined threshold of correlation quality (Mölg et al., in prep.). The authors manually removed single values which would falsify the overall picture, e.g. in the area of strong ice cliff backwasting or proglacial water surfaces. To quantify the uncertainty of the universal kriging interpolation of the velocity point measurements, a semivariogram analysis or a Monte Carlo simulation could have been conducted (Brunsdon and Comber, 2015). This was omitted for lack of time and pressing relevance for the scope of this thesis.

For the debris thickness fieldwork, there is always the possibility of measurement errors. However, since the measurements were always carried out in the same way by the same person, such errors would most likely be systematic and thus would not strongly influence the analysis. Because the thickness measurements for Transect 3 as well as the right limits of Transects 1 and 3 do not stretch all the way to the glacier margin, the debris flux calculated for Flow Units 1 and 3 probably underestimate the actual supraglacial debris flux.

For the statistical analysis, I divide the debris thickness measurements into two categories for the aspect and three categories for the topography. This division is made by hand, as the aspect classification is fairly simple with the notes taken in the field and the DTM of the study area. For the topography classification, an attempt to automatise the division in ArcGIS produced noisy results, which is why the manual approach is used here, too. Therefore, these classifications are dependent on the subjective interpretation of the data.

5. Results

5.1. Debris Origin and Deposition

5.1.1. Rock Walls

The north-facing headwall area above Zmuttgletscher consists either of bare rock wall or is covered with hanging glaciers or perennial snow packs (Fig. C.1). As a result, this area is binarily classified into whether it is bare rock or not. The calculated 3-D areas per accumulation basin are given in Table 3. Headwall 2 has the smallest proportion of rock walls with 47.7 %. For Headwalls 1 and 3, the surface above the glacier predominantly consists of rock walls. Altogether, the headwall above Zmuttgletscher consists of 65 % rock wall.

5.1.2. Deposition Cones and their Contributing Area

The mapping results for the debris deposition cones and their contributing headwall area are shown in Figure 14. A total of 28 cones has been observed: 18 cones for Flow Unit 1, 3 cones for Flow Unit 2 and 7 cones for Flow Unit 3. However, it must be emphasised that Flow Unit 2 has more contiguous and big cones (rather deposition areas than cones, as the whole slope toe is covered by avalanche deposition), while Flow Unit 1 shows predominantly smaller and distinctive and hence more numerous cones. Flow Unit 3 shows both smaller cones as well as one laterally elongated cone.

The calculated contributing areas differ greatly in size and their share of containing rock wall area (Tab. 4). The mean contributing area for the deposition cones for Flow Unit 2 exceeds the mean contributing area for Flow Units 1 and 3 by a factor of 7.4 and 2.7 respectively.

Table 3. Total headwall A_{head} and total rock wall area A_{rock} as well as their ratio A_{rock}/A_{head} in percent. The quantities are given for the three headwall units as well as for the total glacier.

	$A_{head}[m^2]$	$A_{rock}[m^2]$	A_{rock}/A_{head}
Headwall 1	1'297'290	916'455	70.6 %
Headwall 2	1'503'294	716'644	47.7 %
Headwall 3	1'550'368	1'192'858	76.9 %
Total	4'350'952	2'825'957	65.0 %
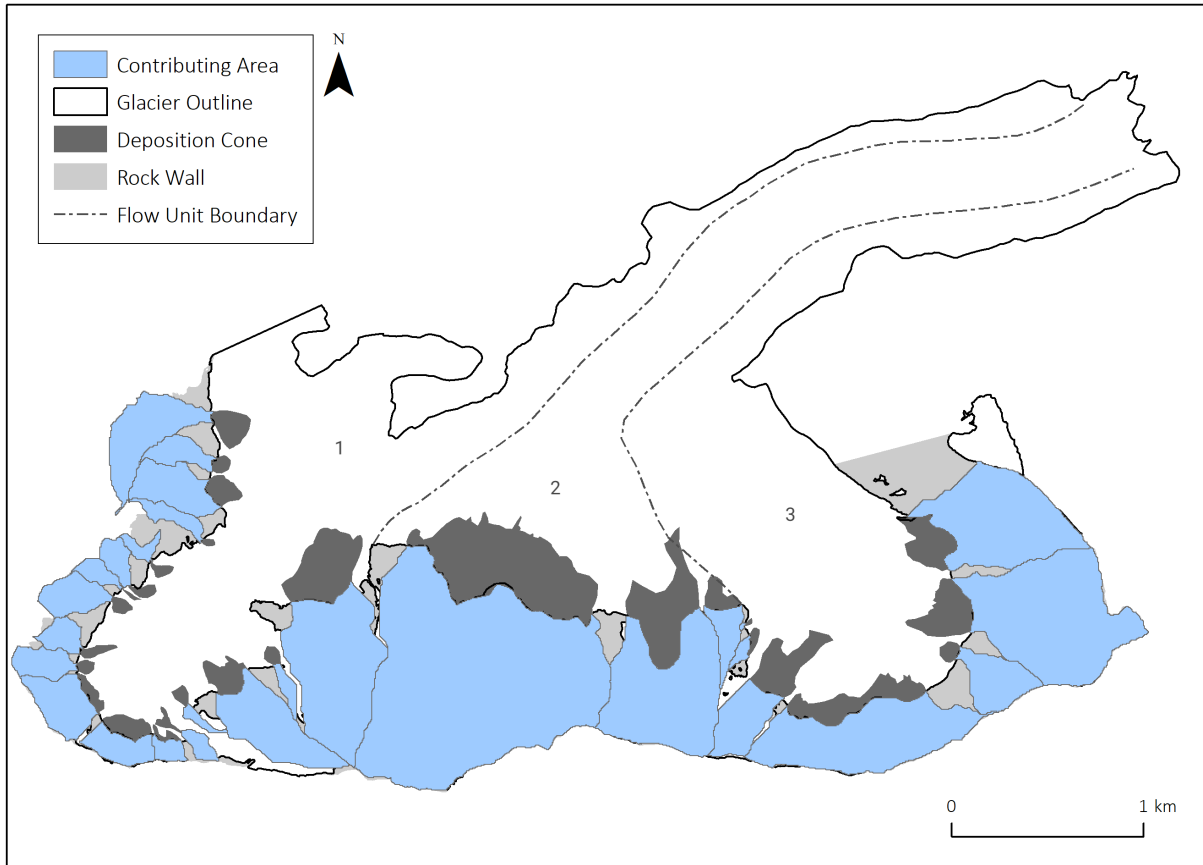
Figure 14. Mapped deposition cones with their respective contributing areas. The three major Flow Units 1 to 3 are displayed with dashed-dotted lines and labelled with their respective number.

Table 4. Number of debris deposition cones, their average contributing areas A_{rock} and their average share of rock wall per contributing area A_{rock}/A_{cont} in percent. The quantities are given for the three headwall units as well as for the total glacier.

	Cones	$\boldsymbol{A_{cont}[m^2]}$	$\boldsymbol{A_{rock}/A_{cont}}$
Headwall 1	18	64'176	65.6 %
Headwall 2	3	475'353	42.2 %
Headwall 3	7	172'996	74.8 %
Total	28	135'436	65.6 %
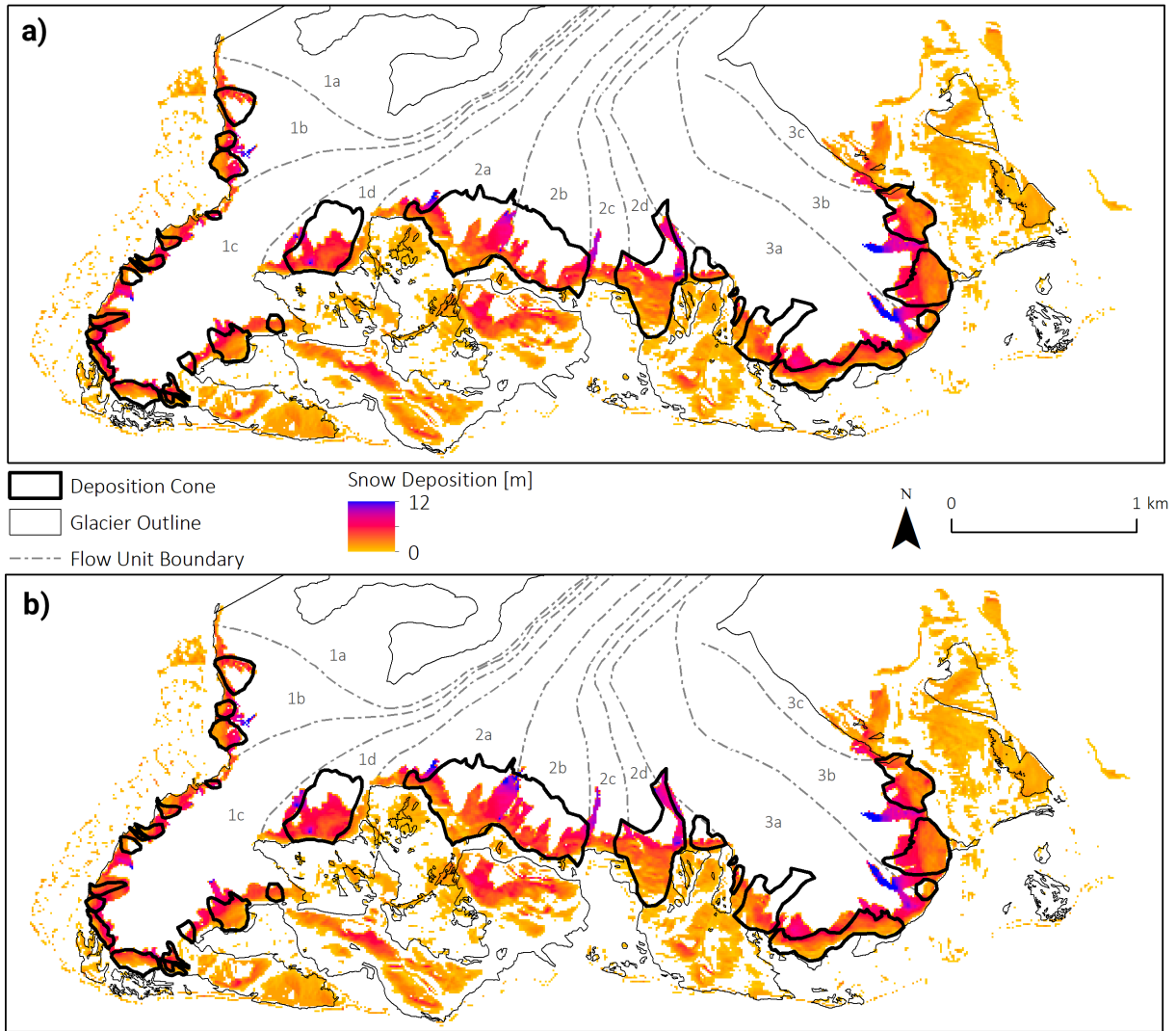
Figure 15. Avalanche snow deposition for the best parameter set $\beta_{lim} = 45°$ and $D_{lim} = 15m$ of the MTD sensitivity analysis. The labels mark the respective flow subunit. a) Avalanche snow deposition from a constant $I = 1m$ for the headwall pixels, b) Avalanche snow deposition from $I = 5m$ for the hanging glacier calving front pixels and $I = 1m$ for the remaining headwall pixels. See Figure C.2 for the two model input maps.

5.1.3. Modelled Reproduction of Deposition Cones

I conducted a sensitivity analysis for the two MTD model parameters β_{lim} and D_{lim}. The model was run with two different input files for the initial mass I, once where the hanging glacier calving fronts were given the same input values as the rest of the headwall ($1\ m$) and once with higher input values for these calving front cells ($5\ m$). The best parameter sets for these two input scenarios are summarised in Table 5. The limiting slope β_{lim} of 45° and the limiting deposition D_{lim} of 15 m produced the most reasonable results.

Figure 15a illustrates the height and expansion of the deposited mass for the scenario with constant initial input mass. The attempt to reproduce the manually mapped deposition cones yields mixed results. On the one hand, some features are very nicely reproduced, such as the elongated debris cone in Flow Unit 2d. On the other hand, however, the MTD model fails to reproduce many big cones, such as in Flow Units 1b, 1c or 3a, and simulates too much deposition

Table 5. Best parameter sets of the limiting slope β_{lim} and the limiting deposition height D_{lim} for the MTD model results displayed in Figure 15. I stands for the initial mass input and I_{HG} for the initial mass input for the hanging glacier calving front pixels (Fig. C.2).

	$I[m]$	$I_{HG}[m]$	$\beta_{lim}[°]$	$D_{lim}[m]$
Figure 15a	1	1	45	15
Figure 15b	1	5	45	15

at other locations, e.g in Flow Unit 1c.

The most striking difference between the visually mapped and the modelled cones are displayed in Flow Units 2a and b, where one big contiguous cone along the slope toe is mapped. Contrary to this, the MTD algorithm produces multiple deposition «fingers» and fails to fill the outline of the cone.

Since Headwall 2 contains a lot of hanging glaciers, my suspicion was that the constant input mass of 1 m of snow fails to reproduce the ice avalanche deposition coming from these calving hanging glaciers, which is supposedly higher than 1 m/a. To take this form of deposition into account, the calving front pixels of four big hanging glaciers have been assigned an input mass of 5 m (Fig. C.2). The result for this simulation is shown in Figure 15b. Now, the cones in Flow Units 1d and 2 are slightly better filled, but the finger-like features are even more emphasised. The model still fails to reproduce the cone-shaped deposition for these areas.

5.1.4. Debris Supply

The debris supply into the glacier system is calculated with the contributing rock wall area multiplied by the erosion rate. The two erosion scenarios produce two different debris supply volumes, summarised in Table 6. Since the debris cones in Flow Unit 1 have the most contributing rock wall area, the debris supply for this area is highest and spans between 124.6 to 2491.7 m^3/a. The contributing rock wall areas for Headwalls 2 and 3 are both of the same magnitude and result in a debris supply range of around 50 to 1000 m^3/a. The comparison with the debris flux (see section 5.3.2) will provide more information about which erosion scenario (minimum or maximum) is more realistic for the glacial system of Zmuttgletscher.

Table 6. Total contributing rock wall area per glacier area A_{rock} and the debris supply S calculated with the two different scenarios $E_{min} = 0.1mm/a$ and $E_{max} = 2mm/a$. The quantities are given for the three major flow units as well as for the total glacier.

	$A_{rock}[m^2]$	$S[m^3/a]$	
		E_{min}	E_{max}
Flow Unit 1	1'245'857.5	124.6	2491.7
Flow Unit 2	507'146.7	50.7	1014.3
Flow Unit 3	534'044.1	53.4	1068.1
Total	2'287'048.3	228.7	4574.1
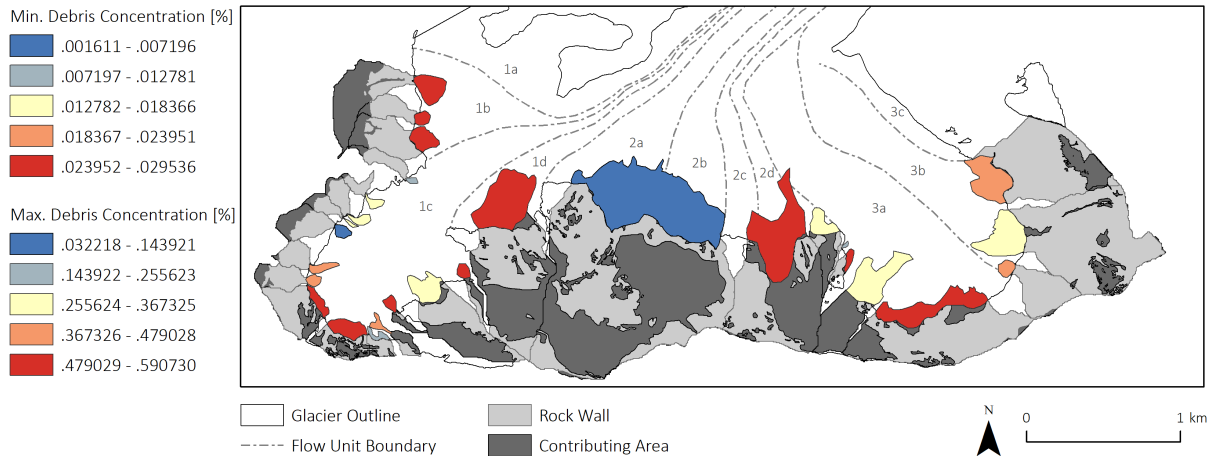
Figure 16. Debris concentration in the deposition cones. The two legends stand for the minimum debris concentration with an erosion input $E_{min} = 0.1mm/a$ and for the maximum debris concentration with an erosion input $E_{max} = 2mm/a$ for the rock wall areas. The five legend classes are divided by equal intervals.

Debris Concentration

The debris concentrations in avalanche-deposited snow per deposition cone are illustrated in Figure 16. The concentrations span between 0.002 and 0.03 % debris in avalanche snow for the minimum erosion scenario and between 0.03 and 0.6 % debris for the maximum erosion scenario. Flow Units 1b and d contain deposition cones which are all very debris-rich, while Flow Unit 1c shows the whole variety of debris concentration. The big contiguous deposition «cone» in Flow Units 2a and b is very debris-poor, owed to the big amount of hanging glacier area in its contributing area. According to my way of calculation, this enters snow and ice into the system, but less debris, lowering the debris concentration. In Flow Unit 2d, however, the debris concentration is increased again. The deposition cones in Flow Unit 3 show average to high debris concentration.

The results for the debris concentration within the glacier ice are calculated only for the three deposition cones in Flow Unit 2. They are not visually presented in a map. For the left, contiguous cone, the concentration spans between 0.005 and 0.1 %; the middle cone generates an englacial debris concentration between 0.08 and 1.6 %; and the right, small deposition cone has a debris concentration ranging between 0.04 and 0.9 % in the glacier ice. Therefore, the overall range for the englacial debris concentration for Flow Unit 2 is from 0.005 to 1.6 %.

5.2. Debris Transport

5.2.1. Flow Units

The flow units resulting from the manual mapping are shown in Figure 17. Zmuttgletscher is formed of the three major Flow Units 1, 2 and 3. Four subunits (a through d) have been observed for Flow Units 1 and 2 respectively, while Flow Unit 3 is composed of three subunits (a through c). Each of the flow units can be traced back to its respective sub-accumulation basin. In the glacier area where the flow unit division is uncertain due to bare ice or snow cover, the

5. Results

flow unit margins are marked with a dashed line.
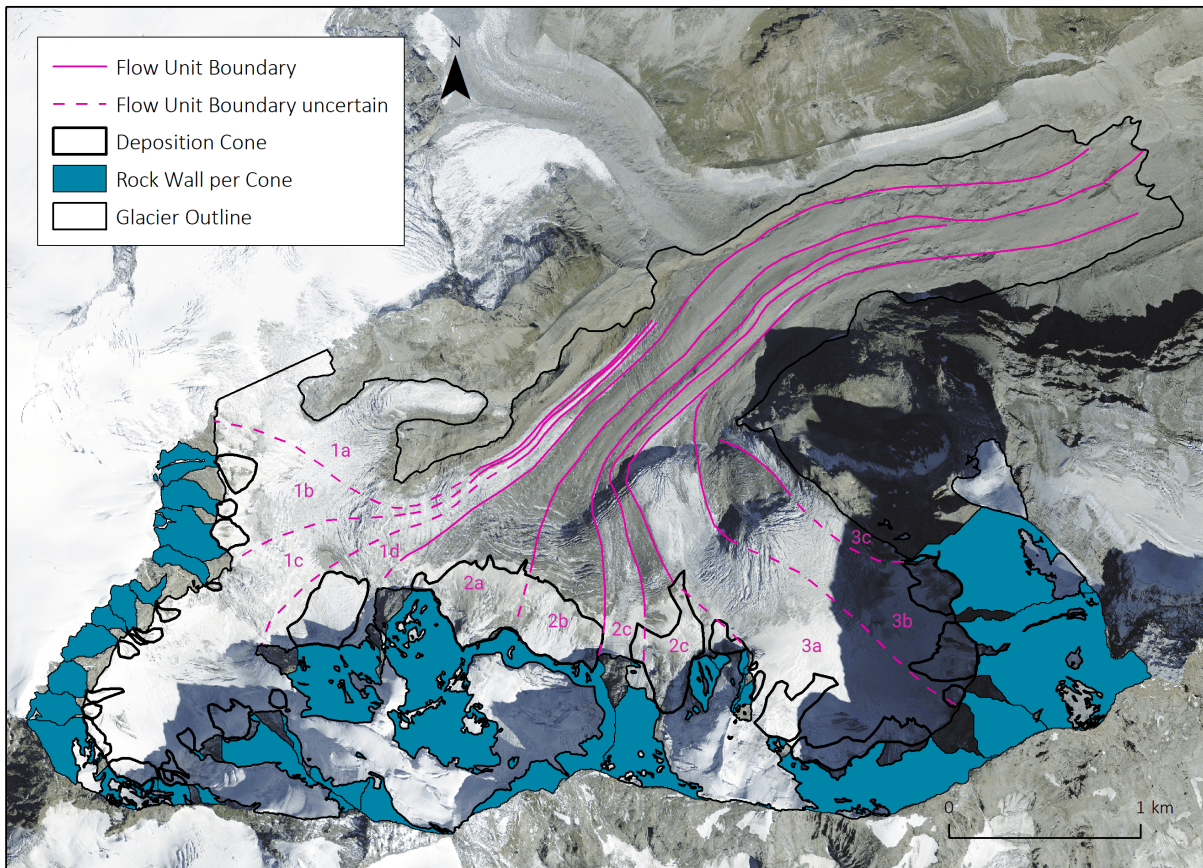
Figure 17. Flow unit division for Zmuttgletscher. The dashed lines mark uncertain flow unit distinction due to bare ice or snow cover. The numbers stand for the respective flow subunit. Furthermore, the deposition cones with their rock wall areas are displayed.

The subunits for Flow Units 1 and 3 are well observable due to the debris melt-out locations, especially in Flow Unit 1, where the four fine subunits closely follow each other and create two distinct debris fingers (see also Fig. 24). However, as soon as the whole major flow units are debris-covered (further down-glacier), their subunit boundaries become very unclear if not impossible to trace, as the glacier is greatly reduced in mass on the glacier margins. Contrary to this, the subunits for Flow Unit 2 are easy to follow down-glacier due to the distinctive rock colours of the debris and the pronounced surface topography. This will allow me to connect the debris thickness measurements within this Flow Unit 2 with their deposition cones with less reservations than for the Flow Units 1 and 3.

5.2.2. Flow Velocities

The interpolation results for the ice flow velocities on the lower glacier tongue are shown in Figure 18. The spatial resolution of one pixel is 2 m. The velocities range from 3 cm/a at the glacier snout up to 14.8 m/a in the middle of Transect 1 and generally decrease towards the margins and the terminus. On the whole, the gradient runs smoothly, except for a sharp boundary between high and low velocities on the left margin of Transect 1. This cut is owed to

limited data points in this area and is probably not accurate. Furthermore, on the right margin of Transect 1, six thickness measuring points are entirely missing velocity interpolation values.
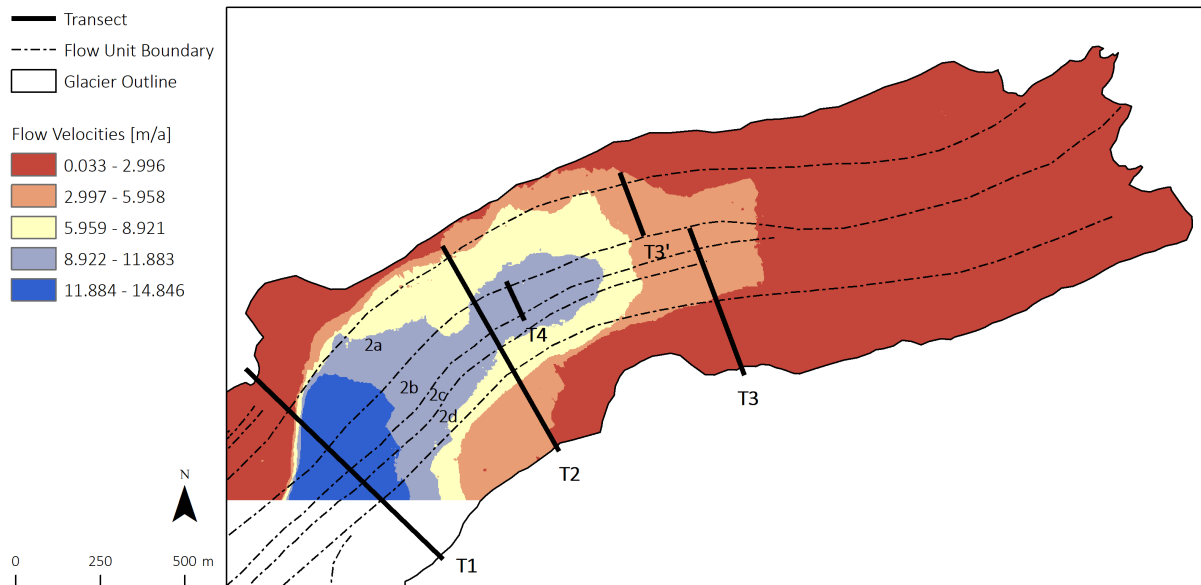
Figure 18. Surface flow velocities on the glacier tongue, interpolated from the point measurement data displayed in Figure B.1 and provided by Mölg et al. (in prep.). The four transects are labelled with T1 trough T4. Furthermore, the four subunits of Flow Unit 2 are marked with their respective number.

The visually mapped flow units are generally well met by flow velocity vectors, as they mostly run parallel to the flow unit margins. However, Flow Units 2c and d are an exception. The flow vectors cross the boundary separating these two subunits from left to right at some locations, implying that the margin there is drawn too far to the left.

5.3. Debris Thickness Distribution

The debris thickness measurements collected for the three cross-section Transects 1 through 3 are illustrated in Figure 19, where both the topography and the thickness measurements are displayed. Where more than one debris thickness measurement per measurement point was taken, the error bars depict the standard deviation of the measurements.

The three cross-section Transects 1 through 3 are presented first, including their statistical analysis and the results for the debris fluxes and emergence rates. Afterwards, the measurement results for Transect 4 are shown (see section 5.3.4).

5.3.1. Cross-Section Transects

Transect 1 shows a relief approaching 30 m with two distinctive crests in the glacial cross-section topography, labelled Crest 1 and Crest 2 in Figure 19a. While the thickness of the debris cover on Crest 1 is quite uniform and thin, the debris on the right side of Crest 2, right underneath the top point, is more than 0.6 m deep and marks the maximum debris thickness for this transect. Also further down the right slope of Crest 2, the debris thicknesses remain high.
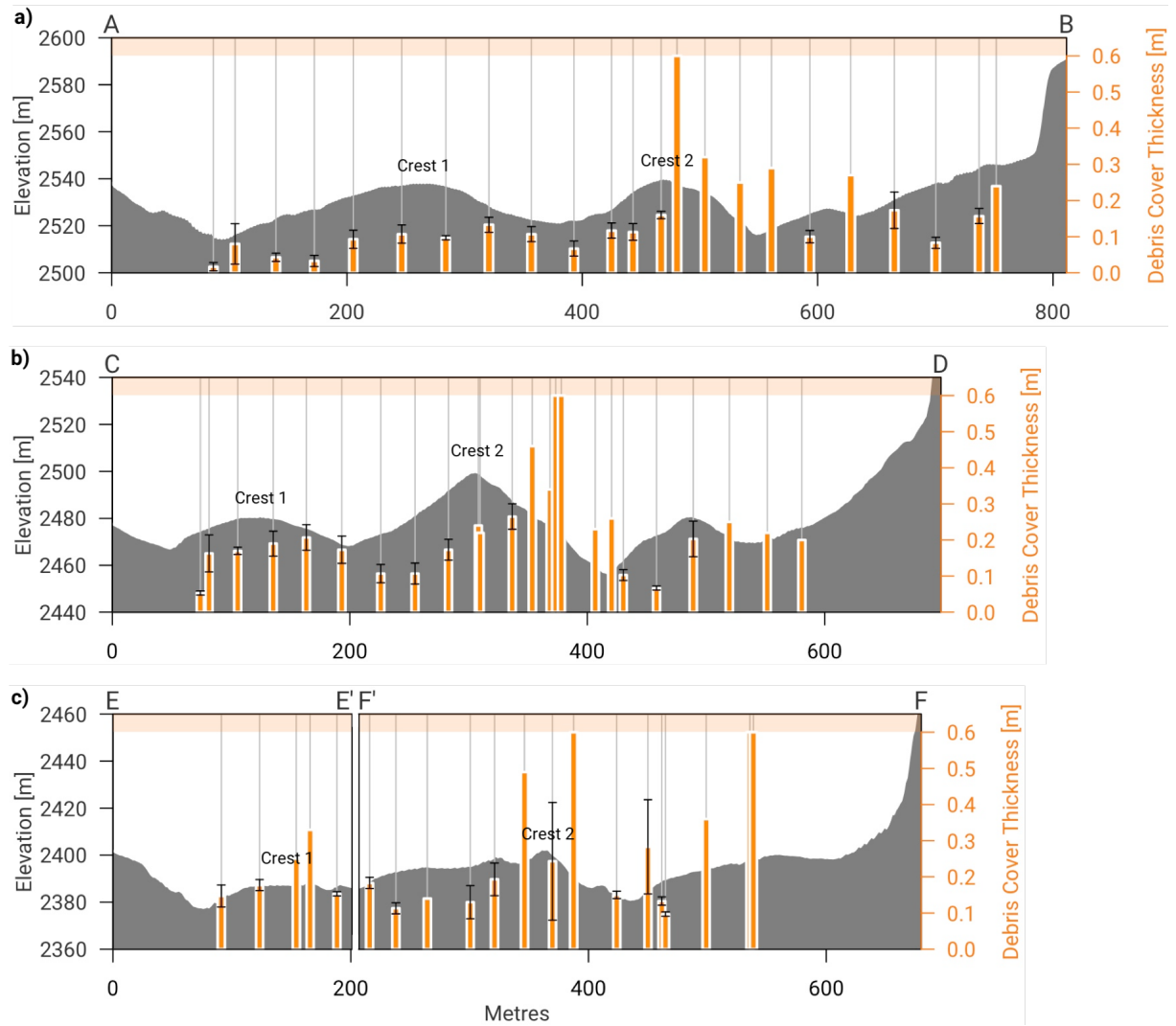
Figure 19. Profile graphs of the three cross-section transects (left y-axis) with the debris thickness measurements indicated in orange (right y-axis). a) Transect 1. b) Transect 2. c) Transect 3. Error bars indicate the standard deviations. The orange bar on top of the graphs marks the digging limit of 0.6 m for the measuring points. The capital letters above the graphs correspond to the transect start and end points marked in Figure 12. Glacier ice flow direction is from the reader away into the page. The two pronounced crests mentioned in section 2 are labelled Crest 1 and Crest 2 respectively. Please note the vertical exaggeration of factor 2 for the elevation.

Further away towards the right glacier margin, the debris is of varying thickness while generally being thicker than on the left glacier margin.

When we connect the topography of Transect 1 with the topography of **Transect 2** down-glacier, the two crests can again be identified. They are labelled in Figure 19b. However, in Transect 2, Crest 1 is less noticeable. The debris cover is again quite uniform over the whole crest, but thicker than for Transect 1. Crest 2 is even more pronounced with a maximum elevation difference of 45 m to the right and again shows much thicker debris on the right slope. However, the debris here is not thickest close to the top but increases towards the middle of the slope (where it again reaches a thickness greater than 0.6 m) and decreases again towards the slope toe.

The debris on the right glacier margin is again thicker than on the left, even though the difference is only slight now. Both margins however are more heavily debris-covered than in Transect 1.

The thickness measurements for **Transect 3** have been taken in an area which is characterised by very rough terrain. Ice cliffs of various heights cut into the surface topography, and Transect 3 had to be interrupted and resumed on two sides of such an ice cliff (as displayed with a cut in Figure 19c).

Crest 1 is not visible anymore in the elevation profile. There are two peaks of higher debris thickness where the crest supposedly would be, but the crest itself is smoothed so far down-glacier. Nonetheless, Crest 2 is still visible with a maximum relief range of 20 m on the right slope. For Transect 3, we now have thick debris on both sides of this crest (0.49 m on the left and more than 0.6 m on the right), while the debris cover on the crest itself with 0.24 m is less marked (even though the error bars emphasise a high spatial heterogeneity). Further towards the right glacier margin, the debris cover thickness increases again to more than 0.6 m.

Statistical Analysis

Generally, one can say with the observations stated above that the debris thickness distribution of Zmuttgletscher is strongly heterogeneous and thus spatially dependent. To investigate the data further than with mere visual analysis, several statistical tests have been conducted. I follow the structure from section 4.3.1 and present the test results for the analysis of the three points (i) gradation, (ii) topography and (iii) variability. The results for the (iv) slope-profile are featured in section 5.3.4.

Gradation

The mean debris thickness measurements per transect including their standard deviation are displayed in Figure 20a. One can observe that the thickness increases towards the tongue of the glacier: We have a mean debris thickness of 0.16 m for Transect 1, 0.23 m for Transect 2 and 0.27 m for Transect 3. However, to test if this trend is also significant concerning the range of the measurements, a test for the comparison of means has to be conducted. Since the three samples of debris thickness are ratio scaled, independent and not normally distributed, a Kruskal-Wallis test was applied and yielded a p-value of 0.02784. As this p-value is below α, the null hypothesis of equality of the mean ranks is rejected. Thus, the debris cover thickness
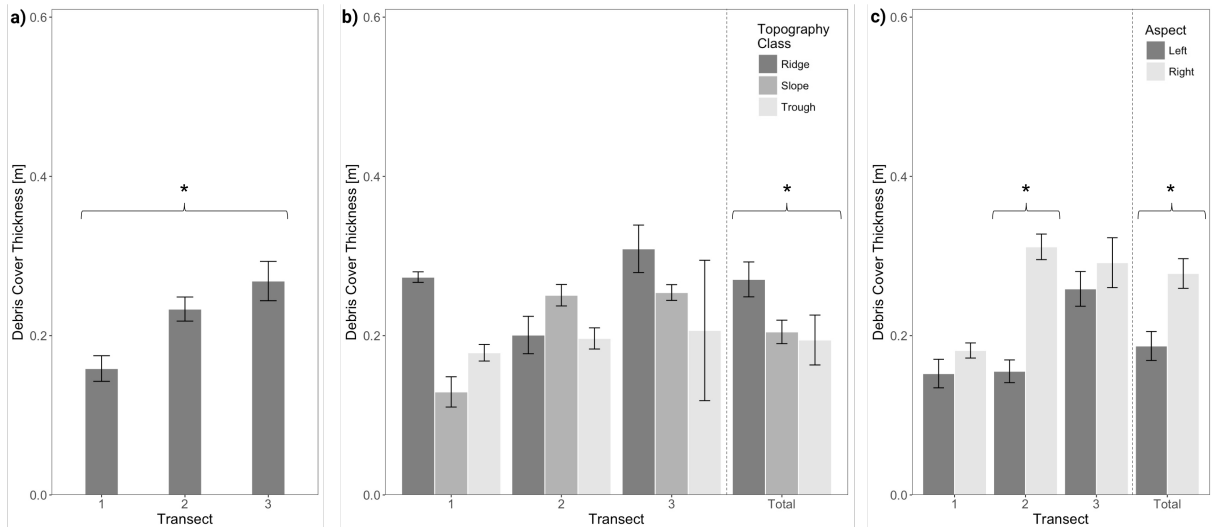
Figure 20. Results of the statistical analysis of the debris cover thickness. a) Mean debris cover thickness per cross-section transect. b) Mean debris cover thickness divided into the three topography classes, both broken down by transect as well as over all cross-section transects (total). c) Mean debris cover thickness divided into the two aspect classes, both broken down by transect as well as over all cross-section transects (total). Error bars show the standard deviations. Statistically significant differences between samples are indicated with a star (*).

statistically significantly varies between the three transects and hence increases towards the glacier tongue.

Topography

To assess whether the surface topography allows to draw any conclusions about the supraglacial debris cover, the three surface features slope, aspect and topography classes have been investigated in terms of their correlation with the debris cover thickness measurements. For the surface **slope**, the two regression lines are shown in Figure 21: the left scatterplot for the surface slope of the measuring points and the right scatterplot for the slope averaged over a 3 m buffer radius around each point.

Already with purely visual estimation, it can be said that the surface slope does not have any influence on the debris thickness distribution, neither for the single-pixel (regression line slope of -0.002) nor for the buffer attempt (regression line slope of 0.001). The coefficients of determination R^2, which describe the proportion of the predicted variance in the total variance and thus the quality of the model, are also very low with 2.1 % for the single-pixel model and 0.4 % for the buffer model. This shows that the surface slope, be it for a single pixel or averaged over a buffer radius of 3 m, is not suited for the prediction of the supraglacial debris cover thickness.

The results for the investigation of the influence of the **aspect** on the debris cover are illustrated in Figure 20c, showing the average values for the total measurements as well as the means per transects. Considering the total amount of the thickness measurements, we have an average debris thickness of 0.19 m for the measurements on the «left» slopes and 0.28 m for the «right» slopes. To test if these two means are significantly different, a Mann-Whitney test was conducted,
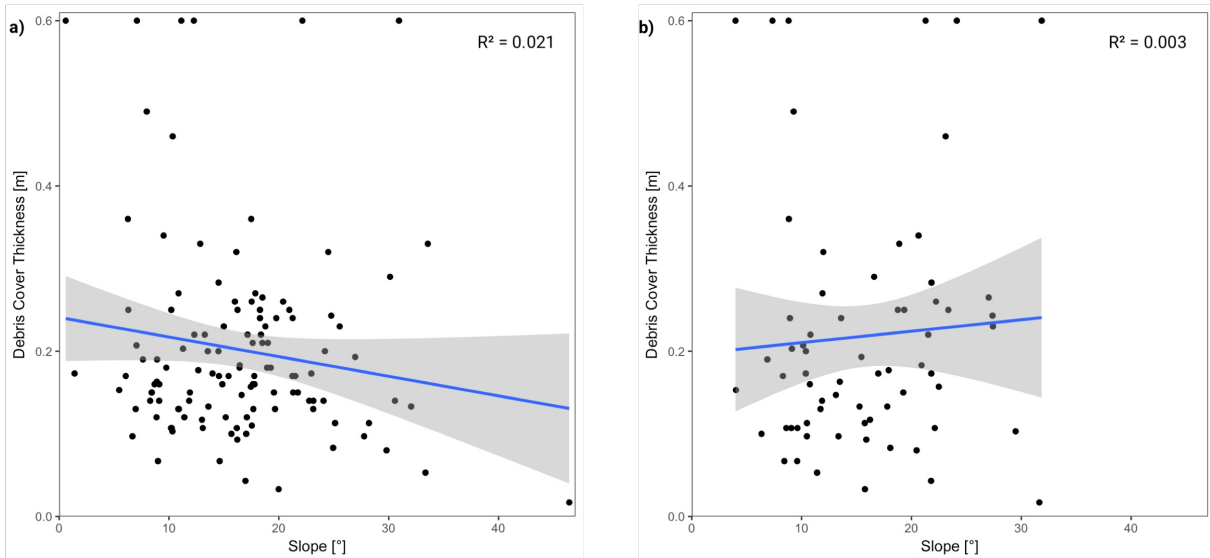
Figure 21. Correlation results of the statistical analysis between the surface slope and the debris cover thickness. a) Debris cover thickness plotted against the surface slope of each measuring point. b) Debris cover thickness plotted against the mean surface slope of a buffer of 3 m around each measuring point. R^2 in the upper right corners is the coefficient of determination for the respective regression model.

as the two samples are ratio scaled, independent and not normally distributed. The test produced a p-value of $0.001134 < \alpha$, and the null hypothesis of equal rank sums is rejected. Hence, the debris cover thickness on the «right» aspects is statistically significantly greater than the thickness on the «left» aspects for the three transects.

When consulting Figure 20c, the clearer thickness difference between the two aspects for Transect 2 compared to Transects 1 and 3 catches the eye. To test for this distinction between the aspects depending on the transects, the same procedure as described above was repeated for the three transects. The Mann-Whitney test for Transect 2 indeed yielded a p-value less than α, while the test results for Transects 1 and 3 produced p-values greater than α. Therefore, the debris cover thickness on the «right» aspects statistically significantly exceeds the thickness on the «left» aspects for Transect 2, while it does not significantly differ for Transects 1 and 3.

The average debris thicknesses divided by the three **topography classes** are displayed in Figure 20b, again illustrating the mean values for all measurements as well as the averages per transects. For the total measurements, the average thickness is 0.27 m for the ridges, 0.21 m for the slopes and 0.20 m for the troughs. The statistical test to support these differences is again the Kruskal-Wallis test, as the three samples are ratio scaled, independent and not normally distributed. The test gave a p-value of $0.02784 < \alpha$, implying that the null hypothesis of equality of the mean ranks must be rejected. Thus, the debris cover thickness on «ridges» is statistically significantly greater than on «slopes», which in turn exceeds the thickness in «troughs».

Figure 20b also displays the different debris thicknesses per topography class divided among the individual transects. However, these differences per transect should be treated with caution, as the sample sizes are rather small, especially for the «trough» class, and they are too small to allow for statistical tests. For the sake of completeness, however, the results are still illustrated.
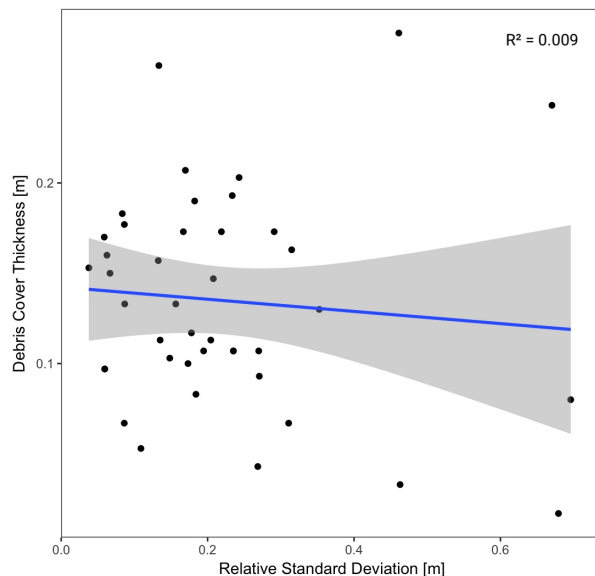
Figure 22. Correlation results of the statistical analysis between the relative standard deviation per measuring point and its debris cover thickness. The relative standard deviation is the standard deviation divided by the average debris thickness to avoid autocorrelation. R^2 is the coefficient of determination for the regression model.

Variability

As already stated multiple times, the thickness of supraglacial debris cover is a highly spatially dependent feature. Since my field measurements also include vast information about the small-scale variability, an investigation of the relation between the relative standard deviation (i.e. the standard deviation per measuring point divided by the mean) and the debris thickness suggests itself. The scatterplot with the regression line is shown in Figure 22, showing neutral results: The regression line slope suggests hardly any correlation between the two quantities (-0.034). The results for the regression analysis (ANOVA) support this result with a very low R^2 of 0.9 %. Therefore, the relative thickness variability is not suitable for predicting the supraglacial debris thickness.

5.3.2. Debris Flux

The results for the calculation of the debris integrals and fluxes for the three transects are presented in Table 7. For both the whole glacier and Flow Unit 2, the debris integrals increase towards the glacier tongue. However, while this increase is quite linear for the whole glacier, the increase in Flow Unit 2 is quite steep between Transects 1 (59.7 m^2) and 2 (79.4 m^2) and then levels off towards Transect 3 (84.0 m^2).

The debris fluxes derived from the integrals and the ice flow velocity are also shown in Table 7. For Flow Unit 2, the debris flux is highest for Transect 1 (759.0 m^3 a^{-1}) and decreases down-glacier to 678.5 m^3 a^{-1} for Transect 2 and then to 360.2 m^3 a^{-1} for Transect 3. The decrease is not linear but more pronounced between the lower two transects. The same applies to the whole glacier area, even though the flux values for Transects 1 and 2 are considerably higher while the flux through Transect 3 is comparable to the one for Flow Unit 2.

Table 7. Debris integral D_{int} and flux Q for the three transects. For the distances between the two transects, the debris emergence rates ER are given.

		$D_{int}[m^2]$	$V[m/a]$	$Q[m^3/a]$	$d[m]$	$ER[mm/100m]$
	Transect 1	98.8	9.744	963.1		
Glacier	Transect 2	106.4	7.551	803.7	570	2.3
	Transect 3	114.0	3.465	395.2	650	2.5
	Transect 1	59.7	12.718	759.0		
Flow Unit 2	Transect 2	79.4	8.549	678.5	570	8.9
	Transect 3	84.0	4.285	360.2	650	1.8

5.3.3. Debris Emergence Rate

With the debris fluxes and the distances between the transects given in Table 7 and the widths of the transects in Table 2, the debris emergence rates between the transects were calculated and are presented in Table 7. Please note that the results are given in $mm/100m$ to present the values more intuitively. While the emergence rates computed for the whole glacier are of nearly the same value, the rate for Flow Unit 2 between Transects 1 and 2 of 8.9 $mm/100m$ considerably exceeds the rate between the lower two transects, which is 1.8 $mm/100m$.

5.3.4. Slope-Profile Transect

The measurement results for the (iv) slope-profile as explained in section 4.3.1, i.e. for left-facing ridge-trough covering **Transect 4**, are presented in Figure 23. Starting from the ridge and going downslope, a general gradual decrease in the debris thickness can be observed. However, the maximum thickness (0.36 m) is not measured on the ridge itself but just below it. Furthermore, when reaching the trough, the debris thickness markedly increases again to 0.33 m.
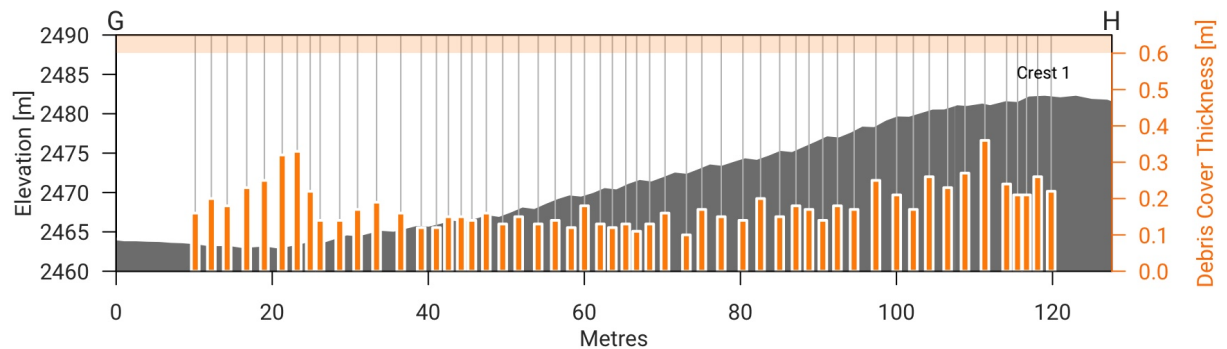
Figure 23. Profile graph of the slope-profile Transect 4 (left y-axis) with the debris thickness measurements indicated in orange (right y-axis). The orange bar on top of the graph marks the digging limit of 0.6 m for the measuring points. The capital letters above the graph correspond to the transect start and end points marked in Figure 12. Glacier ice flow direction is from the reader away into the page. Crest 1 is labelled in the profile. There is no vertical exaggeration applied in this graph.

5. Results

6. Discussion

6.1. Debris Origin and Deposition

Headwall 2 consists of rock wall to a much smaller extent than Headwall 1 or Headwall 3, meaning that there are more hanging glaciers and perennial snow areas. This is owed to the different topography of the three headwall areas, as displayed with the elevation contour lines in Figure 5a or the slope raster map in Figure A.1c. The middle Headwall 2 is less steep, allowing the snow and ice bodies to settle on the wall. The flatter the rock walls, the lower the erosion rates (Hambrey et al., 2008; Anderson and Anderson, 2010). Furthermore, the flatter the rock walls, the more deposited snow and ice in them, and again the lower the erosion rates. As a consequence, the debris concentration in the big contiguous deposition cone below the less steep Headwall 2 is very low.

Anderson and Anderson (2016) have modelled the dynamics of a debris-covered glacier in a numerical glacier model. Since the model simulates in a 2-D space, they assumed a constant value for the debris concentration across the glacier width. However, they emphasise that, in reality, englacial debris concentrations are not uniform because of variable ice flow velocities, snow accumulation rates and debris deposition patterns. For my calculation of the debris concentration in the deposition cones, I took the latter two factors into account. The varying debris deposition patterns and snow accumulations were accounted for by the manual mapping of the cones and the calculation of their contributing area. Even though the snow accumulation rates are uniform with a constant input of 1 m of snow, ignoring slope, aspect and wind redistribution processes, the variable snow input is still accounted for in my thesis. For the varying ice flow velocities, which the authors mention, I argue that they do not have to be considered for the calculation of the debris concentration within the deposition cones. The avalanches forming them come down regularly and build roughly the same deposition extent year by year, independent of the flow velocities of the ice. Hence, I argue that my approximation of the debris concentration within the cones is realistic.

For Flow Unit 2, however, I also calculated the debris concentration within the glacier ice. This glacier part is only fed by avalanches, meaning that its entire accumulation is generated by the deposition cones. The law of mass preservation tells us that the mass of snow stays the same when compacted to ice, but the volume declines. This increases the debris concentration. By taking this compression factor into account, the englacial concentration is calculated. Now

dealing with the debris concentration within the glacier ice, the argument of its dependence on the variable ice flow velocities by Anderson and Anderson (2016) reappears. I suggest that in a glacier area which is only fed by debris-containing avalanches, this component does not have to be considered. For Flow Unit 2, I assume constant debris and snow input by the avalanches with no further accumulation processes. Since the ratio debris–accumulation always stays constant, the concentration is not dependent on the flow velocities. If some subunits flow faster than the others in Flow Unit 2, this means that both debris input and accumulation are reduced in time, not altering the concentration. Hence, I argue that my estimates of the debris concentration within the glacier ice of Flow Unit 2 are reasonable.

This Flow Unit 2 presumably experiences no conventional accumulation anymore. Debris deposited on top of it hence is not transported englacially. Nevertheless, I assume so with my calculations of debris concentration within the glacier ice. This concentration can be thought of as the maximum englacial debris concentration possible for this flow unit. When the debris in this flow unit actually still was embedded in the glacier ice, there was more accumulation than I assume for today for the debris to actually be buried. More accumulation reduces the debris concentration. As this accumulation amount lacks nowadays, my calculated englacial concentration is the maximum for the conditions now prevailing.

Kirkbride and Deline (2013) performed debris concentration measurements in glacier ice on Glacier d'Estelette. They cleared two circles of 10 m and 5 m radius on low-gradient ice on the glacier tongue from debris clasts larger than 1 cm in diameter. At later dates, over melt periods ranging between two days and two years, all clasts appearing within the circles were weighed. With ablation stakes, the mass loss of ice was measured. The ratio of these two quantities yielded the debris concentration. The results vary by two orders of magnitude: 3.0 to 332.9 kg/m^3 for the density of debris in glacier ice were measured. I assume an ice density of 917 kg/m^3 (Cuffey and Paterson, 2010), which gives me a debris concentration range of 0.3 to 36.1 % within the glacier ice. This highly exceeds my results for the maximum debris concentration in glacier ice, which reaches between 0.005 and 1.6 % in Flow Unit 2. Unfortunately, the authors do not make any statements about the precipitation or erosion rates for their study site. Hence, it is not possible for me to discuss this large discrepancy between the concentration values. I argue to heed the authors' measurements with caution, given the vast range of measurement periods.

Even though its contributing area contains fewer rock walls, Flow Unit 2 is sooner (i.e. on a higher elevation) debris-covered compared to the other two glacial units. Bolch (2011) and Anderson and Anderson (2016) state that the englacial debris path and hence the emergence location is controlled by the debris input location. Debris that is deposited far away from the ELA is advected more deeply into the glacier than debris deposited near the ELA, which follows a shallow, short englacial path (Anderson and Anderson, 2016). This is the main reason for the distinction of the three flow units due to their debris emergence location.

Anderson and Anderson (2016) suggest that the location of supraglacial debris deposition relative to the ELA alters the glacier response to debris. The authors observed that constant debris input where ice discharge is high (i.e. near the ELA) leads to longer glaciers with greater fractional debris cover. The same constant debris input where ice discharge is low (i.e. far away from the

ELA) in turn leads to shorter glaciers with smaller fractional debris cover. For Zmuttgletscher, this implies that Flow Unit 2 can stretch longer than the two outer flow units, as the debris thicknesses tend to be higher in the middle than towards the margin (Fig. 19). Glaciers normally stretch longer in the middle than on their margins (Cuffey and Paterson, 2010). The debris input location hence merely acts as an amplification of the glacier geometry of Zmuttgletscher.

The debris supply is controlled by the height, the backweathering rate of the rock walls and the above-glacier catchment geometry (Scherler et al., 2011; Anderson and Anderson, 2016, 2018). In my calculations for the debris supply, I included the former two factors. The height (or rather the 3-D area) of the rock walls represent the potential erosion surface, and the two erosion rate scenarios allow an estimation of the debris input volume range. The glacier catchment geometry was not included, even though the bedrock erosion rates vary depending on the topography: Ridges are eroded more easily than plane surfaces (Heimsath and McGlynn, 2008), and the steeper the rock walls, the higher the erosion (Hambrey et al., 2008; Anderson and Anderson, 2010). For my results, this could imply two things. Either the debris concentration in the deposition cones in area Flow Unit 2, whose headwall is less steep than for Flow Units 1 and 3, is overestimated, or the debris concentration in the other two flow units is underestimated.

Furthermore, the erosion rates are strongly dependent on the lithology and the bedrock fracture density (Anderson and Anderson, 2010; Bolch, 2011), which I did not consider in this study. The varying sediment facies of the debris deposited on the glacier tongue testify of different geological origins (Fig. 11). The constant backweathering rates thus represent a limitation in my approach. However, further research on Zmuttgletscher can work around this limitation with the detailed geological maps available for the headwall of the glacier (swisstopo, 2018).

My debris thickness measurements do not stretch the whole way to the left and right lateral moraine of Zmuttgletscher (Fig. 5a). Therefore, debris supply coming from lateral moraines, which become increasingly unstable as the glacier surface lowers (Hambrey et al., 2008), is not considered here. As observed during our field measurements in September 2017, the outer flanks of the left lateral moraine are generally well vegetated and stable, suggesting that debris transport and deposition occurs almost entirely within these limits for the left glacier margin (Hambrey et al., 2008). On the right moraine (Fig. 7b), there are pronounced debris flow channels, and during fieldwork, we witnessed a small rock fall from the Matterhorn north wall. This suggests that the debris system is not limited by the lateral moraine on the right glacier margin. However, this lateral debris input only influences the thickness distribution on the very glacier margins, which are hardly covered by my measurements.

The three deposition cones in Flow Unit 1b and the single cone in Flow Unit 1d are all classified as very debris-rich cones. This high debris concentration could be the cause for the very fine and distinctive debris emergence bands observed further down-glacier (Fig. 24): Flow Units 1b and d cause the quicker melt-out of the two debris fingers. Flow Units 1a and c with deposition cones containing less debris or no deposition cones in the investigated area at all result in debris emergence locations further down-glacier. This effect is intensified by the further transport distance of englacial debris in Flow Units 1a and c, where the debris input locations are further away from the ELA than for Flow Units 1b and d.

An interesting debris feature shows up on the subunit boundary between Flow Units 1b and

6. Discussion
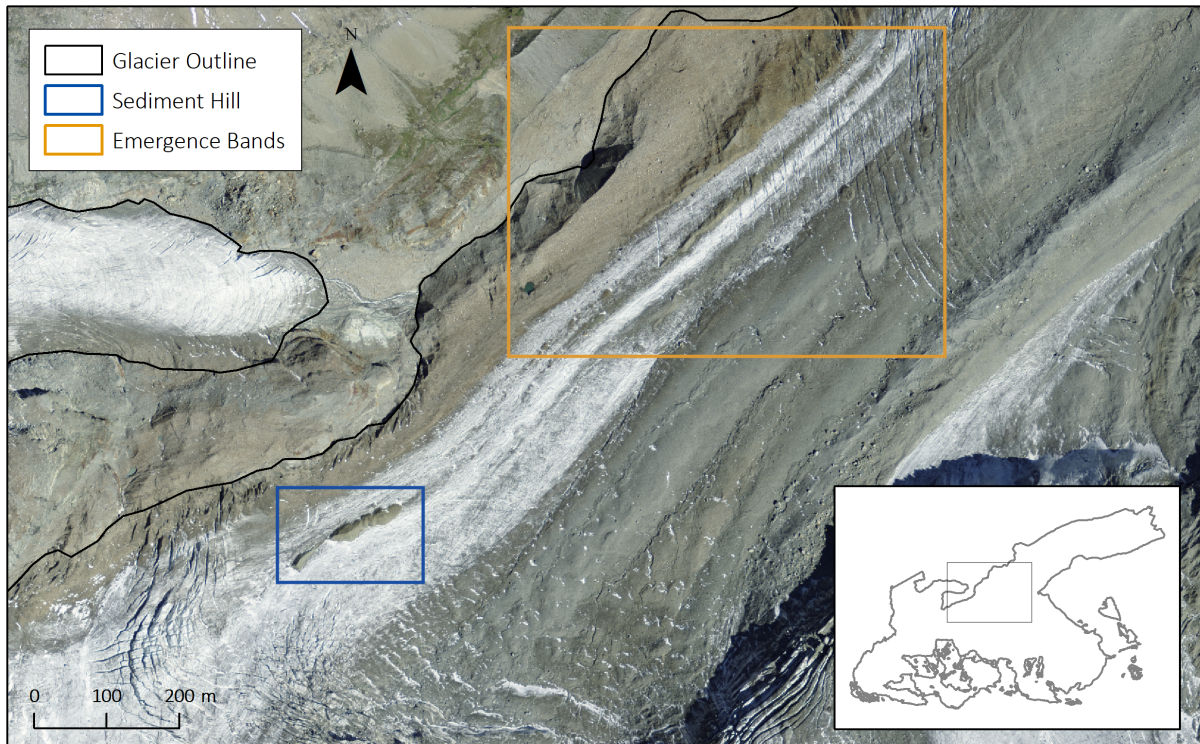
Figure 24. Close-up to the debris emergence location of Flow Unit 1. Sediment hill (blue box) and debris emergence bands of the subunits (orange box). The inset map marks the position of the close-up on the glacier.

c (Fig. 24). An undulant-shaped debris hill of 170 m length emerges from the ice below the crevasses of the big icefall which crosses the whole glacier. Beneath this hill, the ice surface is clean again. Therefore, this is not a typical emergence zone from which the englacial debris is melted out continuously from a debris septum. Even though no single rockfall event was observed on the orthophotographs since 1946, this debris hill suggests that such a rockfall event took place onto Flow Units 1b or c. To determine the approximate period in which this event took place, we would need information about the ice flow velocities up-glacier from this debris hill. The undulating shape might be owed to the arcuate icefall 200 m up-glacier from the hill. Compressional forces down-glacier of the icefall increase flow velocities and the driving stress (Cuffey and Paterson, 2010). When these stresses point into different directions, as it is probably the case beneath this arcuate icefall, they can create surface features with such wavy shapes. This local debris feature demonstrates that single events have a big influence on the small-scale debris concentration in the glacier ice and on the local debris cover thickness. They have to be considered when the supraglacial debris cover is assessed in detail. Furthermore, this sediment hill strongly suggests that the debris concentration within the glacier ice has an influence on the emergence location, as stated by Anderson and Anderson (2016). The deposition zone of this single event cannot deviate strongly from the input locations for the debris originating from constant erosion. Both deposit their sediment at the slope toe of the headwall. This implies the control of the englacial debris concentration on the emergence location.

While the different debris emergence locations for the subunits in Flow Unit 1 can be explained by the different debris concentrations and englacial transport distances, the melt-out patterns

in Flow Unit 3 are not created by the same processes. For this, the transport distances and debris concentrations are too similar between the subunits. The debris emergence location of Flow Unit 3b was the only indicator for the drawing of the subunit boundaries in Flow unit 3. However, it is noticeable that the debris reaches the surface right underneath the other, higher elevated icefall mentioned in the study area description (chapter 2). This is striking, as the flow distances of the three subunits in Flow Unit 3 are of more or less the same and receive comparable debris input from the rock walls. I argue that the debris emergence in Flow Unit 3b is owed to the increased melt in the crevasses of the icefall. Post and LaChapelle (2000) state that, passing through the icefall, the local acceleration stretches out the ice and exposes more area per unit volume. Furthermore, the exposed area is increased by crevassing and fracturing. The ice thus suffers more ablation during the summer melt season. At this local icefall in Flow Unit 3, I suggest that the uppermost debris layer in the ice is very close to the surface. The increased melt in the icefall is enough to melt out the debris sooner than on either sides of the icefall. This results in the supraglacial debris layer beneath this icefall, while the ice is still clean in Flow Units 3a and c.

Most debris on heavily debris-covered glaciers melts out near the point of initial debris emergence where sub-debris melt rates are largest (Anderson and Anderson, 2018). Subsequently, the emergence rates are unlikely to increase towards the terminus: The melt-insulating effects of thickening debris overcomes any increase in englacial debris concentration. This emphasises that once sub-debris melt is negligible, englacial debris no longer emerges so the englacial debris concentration becomes irrelevant. The concentration hence only influences the emergence location (together with the englacial flow path) but not the thickness distribution.

The attempt to reproduce the manually mapped avalanche deposition cones by the MTD algorithm did not produce accurate results. The model does create cone- or rather finger-shaped deposition features, but they hardly meet the «reality» of the mapped cone shapes. A thorough study by Böckli (2008) compared the model performance with the results generated by a physically-based avalanche model (SLF, 2017), and the author concluded that his obtained model results are consistent, which speaks for the MTD algorithm. Nevertheless, I see two model weaknesses for the case study of Zmuttgletscher. Firstly, the DTM used for the model simulation already contains the shape of the deposition cones. This results in the simulated avalanches being deposited on top of the already existing cones. This is probably also the reason why I had to choose a higher value for the maximum deposition slope $\beta_{lim} = 45°$ than the range of 36–41° recommended by Gruber (2007). The second problem is the mass deposition in the headwall. Figure 15 shows that a rather big amount of the initial mass is deposited sooner than at the slope toe of the headwall. Especially in Headwall 2, where the big contiguous cone is poorly filled, there is a lot of headwall deposition. Böckli (2008) states that the alpine landscape is covered by snow in winter, smoothing out the actual topography. This circumstance is not accounted for with the DTM used as input, which could be the reason for this headwall deposition. Unfortunately, the model has no function which prohibits deposition in the area which is generating the mass input. If it did, the amount of deposited material in the headwall would be added to the deposition cones. Most cones which are badly filled by the model have a lot of headwall deposition in their contributing area, especially in Headwall 2. If this deposit

was not possible, these cones would be better filled.

6.2. Debris Transport

Typically, valley glaciers have complex pathways that are related to the structural evolution of the glacier (Hambrey et al., 2008). Zmuttgletscher is composed of two big accumulation basins (Flow Units 1 and 3) which still experience conventional mass gain by precipitation, and one glacier segment (Flow Unit 2) where accumulation happens presumably exclusively by avalanching. The flow unit boundaries have been assessed based on the supraglacial debris emergence patterns, the debris colour and the surface topography: The distinction of the glacier into the three major Flow Units 1, 2 and 3 was based on the emergence locations, while the division of the subunits included all three mentioned criteria.

The subunits for Flow Units 1 and 3 are well visible by their emergence locations but are not traceable anymore once the debris has actually started to melt out. For Flow Unit 2, the division into the four subunits was possible all the way down-glacier to Transect 3. This distinction was primarily based on the debris colour, as there are colourful debris bands visible for this glacier part (Fig. 11). Anderson (2000) and Gibson et al. (2017) state that glaciers with multiple accumulations basins tend to form ice stream interaction medial moraines. This implies that distinctive longitudinal crests on debris-covered glacier tongues describe flow unit boundaries. The boundaries resulting from the distinctive debris colour, however, are not all the way consistent with the surface topography. Beneath the glacier-wide icefall until Transect 1, the colour boundaries enclose the two Crests 1 and 2. Further down-glacier, at Transect 2, the subunit boundary between Flow Units 2b and c has shifted to the right, now actually running on Crest 2. And at Transect 3, the boundaries between Flow Units 2b and c as well as between Flow Units 2c and d have again shifted to the left, now running along left from Crest 2.

This inconsistency of debris colour and surface topography suggests that it is difficult to trace the flow units from the debris-covered glacier part up to the headwall, even if the whole glacier part is debris-covered. This is nicely displayed in Flow Unit 2b. This subunit consists of distinctive red sediment, and one could think that it is easily traced back up-glacier to its lithological origin. However, the flow units derived by the debris colour, as done in this study, do not match the surface topography. This suggests that neither the debris colour nor the surface topography allow to unreservedly divide Zmuttgletscher into its transport pathways for the entirely debris-covered Flow Unit 2.

Anderson and Anderson (2018) emphasise that ice velocity fields control the trajectories of debris-covered ice. Since the two criteria debris colour and surface topography do not produce matching unit boundaries, the comparison of the manually mapped flow units to the vector field is crucial. The flow units derived from the debris colour bands agree well with the vector field, except for the boundary between Flow Units 2c and d, which should have been slightly further to the right. Overall, there is a high consistency between the flow units and the vector field. This suggests that for Zmuttgletscher, the bands of different debris colours are better suited to determine the flow units than the surface topography.

Hambrey et al. (2008) suggest that the bedrock geology is relevant for discriminating transport paths through the glaciers and defining flow unit boundaries. Hence, to estimate the mapped

flow units for Zmuttgletscher conclusively, lithological samples can be compared to the geological map of the headwall above the glacier (swisstopo, 2018).

The interpolation results for the flow velocities obtained by universal kriging show very low surface velocity gradients on the lower part of the glacier tongue. The lowest kilometre of the glacier shows flow velocities of less than 3 m/a and can be considered as almost stagnant. This meets previous observations on debris-covered glaciers, where reversed ablation gradients on the glacier tongue cause reduced driving stresses (Benn et al., 2012). This favours glacier slowdown and subsequent stagnation (Quincey et al., 2009), independent of climate warming (Scherler et al., 2011; Konrad and Humphrey, 2000; Anderson and Anderson, 2016). Hence, I argue that the velocity point measurement interpolation is a suitable component to the assessment of the supraglacial debris cover on Zmuttgletscher.

6.3. Debris Thickness Distribution

Anderson and Anderson (2018) emphasise that the supraglacial debris thickness patterns are controlled by two factors: ablation and flow velocity. These two factors counterbalance each other in terms of their influence on the debris cover, but not perfectly. The more melt and hence ablation we have, the thicker the debris gets. But the faster the ice flows, the thinner the debris cover becomes. These inverse effects determine the debris cover thickness distribution along the glacier.

For the explanation of the supraglacial debris cover of Zmuttgletscher, I neglect the local effects of surface streams, surface lakes, thermokarst and ice cliffs that lead to complex local topography and melt rates. Though they are important for the current downwasting of debris-covered glaciers (e.g. Buri et al., 2016), they play a secondary role in controlling debris thickness patterns (Anderson and Anderson, 2018). Supraglacial debris thickness distribution is rather controlled by debris emergence patterns and surface velocity gradients (Nakawo et al., 1986; Kirkbride and Warren, 1999; Anderson and Anderson, 2016, 2018), which I both include in the discussion of my results.

The calculated emergence rate gradients differ depending on whether the whole glacier or only Flow Unit 2 are considered (Tab. 7). When the whole glacier is accounted for, the emergence rate stays almost constant, while it decreases down-glacier in Flow Unit 2. Anderson and Anderson (2018) express that, as debris thickness increases towards the tongue, the melt is reduced and the emergence rate declines towards the terminus. Based on this statement, I support my analysis with the decreasing emergence rate in Flow Unit 2, since the emergence rates for the whole glacier are unrealistic. A possible reason for these strange results could be the average width between two transects I use for the calculation of the emergence rates. They vary quite strongly for the whole transects (see Tab. 2), which influences the computed emergence rates across the entire glacier.

The initial formation of a debris cover out of longitudinal debris septa is nicely observable in Flow Unit 1 (Fig. 24). Inhibited ablation along a septum outcrop reduces surface lowering and causes a crest relief which increases downstream (Kirkbride and Deline, 2013). Lateral debris motion down the slopes widens the crest, and when adjacent crests coalesce, a complete debris debris cover is formed (Anderson, 2000). Supraglacial debris thickness increases down-glacier

6. Discussion

(e.g. Nakawo et al., 1986; Kirkbride, 1993; Kirkbride and Warren, 1999; Owen et al., 2003; Zhang et al., 2011; Juen et al., 2014; Schauwecker et al., 2015; Anderson and Anderson, 2016). This is owed to two reasons. Firstly, the glacier surface in the ablation zone acts like a conveyor belt: Debris can only be added as it is advected toward the terminus, not removed. Secondly, the surface velocities tend to monotonically decline towards zero, which means that more debris is transported into a fixed cell than is transported out (Anderson and Anderson, 2018). The increasing debris cover thicknesses down-glacier are also observable on Zmuttgletscher, as Figure 20a shows, owing to the decreasing velocities (Fig. 18) which counteract the reduced debris emergence rates (Tab. 7).

The debris thickness patterns across the glacier width have been assessed on the seven debris-covered Bara Shigri, Rakhiot, Khumbu, Koxkar, Panchi Nala, Qingbingtan and Venerocolo glaciers, which show thin debris in the glacier centre, with thicker debris away from the centre and then thinner debris again near the glacier margin (Owen et al., 2003; Juen et al., 2014; McKinney, 2014; Bochiola et al., 2015; Schauwecker et al., 2015; Garg et al., 2017; Wang et al., 2017; Huang et al., 2018). Debris thinning on the final descent to the glacier edge could be the result of divergent flow and the typical convex-up transverse surface profile observed on valley glaciers (Anderson and Anderson, 2018). These characteristics are not directly applicable to Zmuttgletscher. In general, the debris cover is thickest in the glacier centre and declines towards the margins (Fig. 19). This is probably because Flow Unit 2 in the centre of the glacier transports debris that was directly deposited on the glacier without englacial transport. This leads to a thicker debris cover compared to Flow Units 1 and 3, where the debris first has to melt out. The thickness decline towards the glacier edges observed on above-mentioned seven glaciers is less pronounced on the right margin of Zmuttgletscher. The north wall of Matterhorn still generates inputs from the side (especially in Transect 3).

Glaciers with multiple accumulations basins (e.g. Jennings et al., 2014) tend to form ice stream interaction medial moraines (Anderson, 2000; Gibson et al., 2017). The two Crests 1 and 2 might be medial moraines, but it is not possible to evaluate with the data provided for this thesis. Such merging debris-covered tributaries may lead to across-glacier debris thickness variations. This would imply that the surface morphology of upper Transect 1 can be explained by the debris thickness, since the debris cover is still quite «fresh» and has not undergone gravitational redistribution processes yet. Figure 20b shows that the debris is thickest on the ridges for this upper transect, supporting the medial moraine concept mentioned above. Where ice cliff-rimmed supraglacial ponds develop, the typical debris thickness on elevated areas is of the order of 1 m (Hambrey et al., 2008). Transect 3 was taken in an area where ice cliffs with such ponds occur. However, the debris thickness measurements for this transect are not everywhere in this order of magnitude (e.g. not Crest 2). The surface morphology down-glacier, where Transect 3 is situated, is explained by additional processes, e.g. gravitational redistribution processes. The thick debris on the crests is sliding down into depressions. Subsequently, the debris gets thicker in depressions. This slows ablation in the troughs and leads to less surface lowering in the depressions than for the areas surrounding the troughs. This process is called topography inversion, with depressions becoming elevated areas and vice versa (Hambrey et al., 2008). Kirkbride and Deline (2013) state that a debris cover tends towards a layer of uniform

thickness, which is likely the reason for the down-glacier disappearance of Crest 1. Such surfaces are often referred to as thermokarst (Gulley and Benn, 2007). Figure 20b displays the topography inversion effect nicely. The average thicknesses for the three investigated topography classes seem to change randomly between the three cross-section transects. Transect 4 (Fig. 23) also illustrates this ongoing redistribution process: Debris thickness is high both on the ridge and in the trough. It is possible that the thick debris on the ridge is still a remnant of the ice stream interaction which already shows some gravitational redistribution (the maximum lies right underneath the ridge). The thick debris in the trough is a result of this process and will inhibit melt. Hence, this slope-profile is prone to be inverted gradually in time.

The debris thickness on Zmuttgletscher also depends on the aspect relative to the flow direction, for the whole glacier as well as all three individual transects (Fig. 20c). The slopes to the right have consistently thicker debris than the left slopes. This might be owed to the exposition to the sun. The right aspect points to the south and south-east. Even though the debris insulates the underlying ice (Østrem, 1959; Nicholson and Benn, 2006), the constantly higher energy input on the right slopes compared to the left could cause more debris to melt out from the ice.

Contrary to the aspect, the slope has no control on the thickness patterns. I argue that this is owed to the topography inversion effect. Since the topography classes «ridge», «slope» and «trough» are directly dependent on the surface slope, the topography has just as little control over the debris thickness as the slope itself does. The same applies to my analysis of the small-scale variability of the debris thickness. The variety of processes leading to the small-scale thickness variations makes it impossible to predict the thickness with said variations.

Debris-covered glacier length is highly sensitive to debris flux on the glacier surface (Anderson and Anderson, 2016). Responding to the same climate, high surface debris fluxes increase glacier lengths relative to clean ice glaciers. The higher the debris flux, the longer the debris-covered glacier. A high debris flux either implies high flow velocities, allowing the glacier to reach further, or it implies a thick debris mantle, insulating the ice and allowing the glacier to reach further than it would without the debris mantle. Debris flux generally decreases down-glacier, causing the typical stagnating and concave-shaped, elongated glacier tongue (Anderson and Anderson, 2018). This is met by my data, where the debris flux gradually decreases for the three investigated transects. Since the debris integral increases down-glacier, the flux decline must primarily be controlled by the decreasing flow velocities towards the glacier tongue. Further factors governing the debris flux, such as the debris deposition zone width or the debris deposition rate are of secondary importance for determining the glacier geometry (Anderson and Anderson, 2016).

The debris supply volume for Flow Unit 2 ranges between 50.7 and 1014.3 m^3/a (Tab. 6). The debris flux through Transect 1, which is the flux closest to the entrainment zone and hence best suited for the comparison with the debris supply, is 759.0 m^3/a for this flow unit. Given that the supraglacial debris flux always underestimates the actual debris flux, which includes the englacial debris (see e.g. Heimsath and McGlynn, 2008), the maximum erosion scenario with a debris input volume of 1014.3 m^3/a fits the debris flux calculation. This implies that the 2 mm/a scenario for the erosion rates applies best to my calculations.

6.4. Synthesis

Supraglacial debris cover is the result of three components: debris origin and deposition, debris transport and debris thickness distribution. These three factors form a connected system. When assessing a debris cover, all factors must be considered to create a holistic framework.

Debris enters the glacial system of Zmuttgletscher primarily via avalanche deposition cones. Depending on the topography of the headwall, eroded material is deposited onto the glacier. The steeper the headwall, the less likely are perennial snow patches or hanging glaciers, and the more bare rock wall is available for erosion. Hence, deposition cones contain the more debris relative to the avalanche-deposited snow, the more relative amount of rock wall area they possess in their contributing area.

Depending on where the avalanches come down (Flow Unit 1, 2 or 3), debris passes through different paths. On the one hand, debris is englacially embedded in the ice and melts out further down-glacier. This is the case for Flow Units 1 and 3. The debris emergence zone is controlled by the distance between the deposition zone and the ELA and the debris concentration within the ice. The influence of the deposition distance relative to the ELA is explained by the glacier dynamics schematically displayed in Figure 2. The influence of the debris concentration is illustrated by the sediment hill in Figure 24.

On the other hand, debris is deposited onto the glacier beneath the ELA and is only transported supraglacially. This is the case for Flow Unit 2. As a consequence, the debris cover in Flow Unit 2 is generally thicker than in Flow Units 1 and 3, where the debris first has to melt out.

The spatial distribution patterns of the debris cover are largely in line with previous research observations and simulations. Where they are not, possible reasons for limitations in the calculation explain the deviations. Well established concepts, such as the decreasing debris emergence rate towards the glacier snout or the topography inversion effect, are supported by the field measurements and data analysis. New observations, such as the correlation between aspect and debris thickness, again impressively underline the potential of this field of research.

To combine debris thickness patterns on glacier tongues with the debris input conditions and locations further up-glacier, particular attention must be paid to the correct determination of the glacial flow units. Only then, integral conclusions about the evolution of a supraglacial debris mantle are possible.

7. Conclusion

Debris covers are a mystery still to be uncovered. Their contradictory effects on glacier melt and dynamics are extensively researched, but not yet understood. In this thesis, I confirm previous observations and model results made for the supraglacial debris cover on valley glaciers by new measurement series taken at and applied to Zmuttgletscher, a new study site. This study shows that the particular topography and climate are crucial to debris cover analysis when applying simulation results to the real world. The site-specific links between headwall and flow units or the course of the ELA strongly influence the shape of the supraglacial debris mantle.

I believe that thoroughly executed, debris thickness measurement campaigns can complement and extend other existing efforts to understand the evolution of debris-covered glaciers. This study offers, to the best of my knowledge, the first collection of extensive debris thickness measurements combined in a holistic analysis of the debris mantle. This integral assessment of Zmuttgletscher allows to set observations of supraglacial debris cover – not least of all the ones deviating from literature – into relation with its origin and pathways. While being confined to the study area, the results and observations extracted from this study still help to better understand the influence of supraglacial debris on glacier melt and dynamics.

Bibliography

Anderson, L. S. and Anderson, R. S. (2010). *Geomorphology: The Mechanics and Chemistry of Landscapes*. Cambridge University Press. 43, 45

Anderson, L. S. and Anderson, R. S. (2016). Modeling debris-covered glaciers: response to steady debris deposition. *The Cryosphere*, 10:1105–1124. 3, 4, 43, 44, 45, 46, 49, 50, 51

Anderson, L. S. and Anderson, R. S. (2018). Debris thickness patterns on debris-covered glaciers. *Geomorphology*, 311:1–12. 2, 3, 45, 47, 48, 49, 50, 51

Anderson, R. S. (2000). A model of ablation-dominated medial moraines and the generation of debris-mantled glacier snouts. *Journal of Glaciology*, 46(154):459–469. 21, 48, 49, 50

Bakke, J. and Nesje, A. (2011). Equilibrium-line altitude (ELA). In Singh, V. P., Singh, P., and Haritashya, U. K., editors, *Encyclopedia of Snow, Ice and Glaciers*, pages 268–277. Springer. 1

Basnett, S., Kulkarni, A., and Bolch, T. (2013). The influence of debris cover and glacial lakes on the recession of glaciers in Sikkim Himalaya, India. *Journal of Glaciology*, 59(218):1035–1046. 4

Benn, D. I., Bolch, T., Hands, K., Gulley, J., Luckman, A., Nicholson, L. I., Quincey, D., Thompson, S., Toumi, R., and Wiseman, S. (2012). Response of debris-covered glaciers in the Mount Everest region to recent warming, and implications for outburst flood hazards. *Earth-Science Review*, 114:156–174. 2, 4, 5, 49

Bochiola, D., Senese, A., Mihalcea, C., Mosconi, B., D'Agata, C., Smiraglia, C., and Diolaiuti, G. (2015). An ablation model for debris-covered ice: the case study of venerocolo glacier (Italian Alps). *Geografia Fisica e Dinamica Quaternaria*, 38(2):113–128. 4, 50

Böckli, L. (2008). *Modellierung der Ablagerung von kleinen, häufigen Lawinen*. PhD thesis, Geographisches Institut, Universität Zürich. 19, 20, 47

Bolch, T. (2011). Debris. In Singh, V. P., Singh, P., and Haritashya, U. K., editors, *Encyclopedia of Snow, Ice and Glaciers*, pages 186–188. Springer. 2, 3, 5, 6, 17, 27, 44, 45

Bibliography

Bolch, T., Kulkarni, A., A.Kääb, Huggel, C., Paul, F., Cogley, J. G., Frey, H., Kargel, J. S., Fujita, K., Scheel, M., Bajracharya, S., and Stoffel, M. (2012). The State and Fate of Himalayan Glaciers. *Science*, 336(6079):310–314. 5

Bolch, T., Pieczonka, T., and Benn, D. I. (2011). Multi-decadal mass loss of glaciers in the Everest area (Nepal Himalaya) derived from stereo imagery. *The Cryosphere*, 5(2):349–358. 5

Bozhinskiy, A. N., Krass, M. S., and Popovnin, V. V. (1986). Role of debris cover in the thermal physics of glaciers. *Journal of Glaciology*, 32:255–266. 4

Brock, B. W., Mihalcea, C., Kirkbride, M. P., Diolaiuti, G., Cutler, M. E. J., and Smiraglia, C. (2010). Meteorology and surface energy fluxes in the 2005-2007 ablation seasons at the Miage debris-covered glacier, Mont Blanc Massif, Italian Alps. *Journal of Geophysical Research*, 115(D9). 5

Brunsdon, C. and Comber, M. (2015). *An introduction to R for spatial analysis and mapping.* SAGE. 28

Buri, P. (2017). *Understanding the role of ice cliffs on ablation patterns and mass balance of debris-covered glaciers in a Himalayan catchment.* PhD thesis, Institute of Environmental Engineering, ETH Zürich. 5

Buri, P., Pellicciotti, F., Steiner, J. F., Miles, E. S., and Immerzeel, W. W. (2016). A grid-based model of backwasting of supraglacial ice cliffs on debris-covered glaciers. *Annals of Glaciology*, 57:199–211. 49

Carenzo, M., Pellicciotti, F., Mabillard, J., Reid, T., and Brock, B. (2016). An enhanced temperature index model for debris-covered glaciers accounting for thickness effect. *Advances in Water Resources*, 94:457–469. 5

Cuffey, K. M. and Paterson, W. S. B. (2010). *The physics of glaciers.* Elsevier, 4th edition edition. 21, 44, 45, 46

de Haas, T., Conway, S. J., and Krautblatter, M. (2015). Recent (Late Amazonian) enhanced backweathering rates on mars: Paracratering evidence from gully alcoves. *Journal of Geophysical Research: Planets*, 120(12):2169–2189. 7, 18

Deline, P. (2005). Change in surface debris cover on Mont Blanc massif glaciers after the Little Ice Age termination. *The Holocene*, 15(2):302–309. 2, 12

Dobhal, D. P. (2011). Glacier. In Singh, V. P., Singh, P., and Haritashya, U. K., editors, *Encyclopedia of Snow, Ice and Glaciers*, pages 376–377. Springer. 1

Foster, L., Brock, B., Cutler, M., and Diotri, F. (2012). A physically based method for estimating supraglacial debris thickness from thermal band remote-sensing data. *Journal of Glaciology*, 58(210):677–691. 5

Gardelle, J., Berthier, E., and Arnaud, Y. (2012). Slight mass gain of Karakoram glaciers in the early twenty-first century. *Nature Geoscience*, 5(5):322–325. 4

Gardelle, J., Berthier, E., Arnaud, Y., and Kääb, A. (2013). Region-wide glacier mass balances over the Pamir-Karakoram-Himalaya during 1999-2011. *The Cryosphere*, 7(4):1263–1286. 4

Gardner, A. S., Moholdt, G., Cogley, J. G., Wouters, B., Arendt, A. A., Wahr, J., Berthier, E., Hock, R., Pfeffer, W. T., Kaser, G., Liegtenberg, S. R. M., Bolch, T., Sharp, M. J., Hagen, J. O., van den Broeke, M. R., and Paul, F. (2013). A reconciled estimate of glacier contributions to sea level rise: 2003 to 2009. *Science*, 340(6134):852–857. 5

Garg, P. K., Shukla, A., Tiwari, R. K., and Jasrotia, A. S. (2017). Assessing the status of glacier in part of the Chandra basin, Himachal Himalaya: a multiparametric approach. *Geomorpholgy*, 284:99–114. 2, 4, 50

Gibson, M. J., Glasser, N. F., Quincey, D. J., Mayer, C., Rowan, A. V., and Irvine-Flynn, T. D. L. (2017). Temporal variations in supraglacial debris distribution on Baltoro Glacier, Karakoram between 2001 and 2012. *Geomorphology*, 295:572–585. 21, 48, 50

GLAMOS (2018). Swiss glacier monitoring network. 12

Gruber, S. (2007). A mass-conserving fast algorithm to parameterize gravitational transport and deposition using digital elevation models. *Water Resources Research*, 43(6). 18, 19, 27, 47

Gulley, J. and Benn, D. I. (2007). Structural control of englacial drainage systems in Himalayan debris-covered glaciers. *Journal of Glaciology*, 53(182):399–412. 51

Haeberli, W. (2011). Glacier mass balance. In Singh, V. P., Singh, P., and Haritashya, U. K., editors, *Encyclopedia of Snow, Ice and Glaciers*, pages 399–408. Springer. 1

Haeberli, W., Wegmann, M., and Mühll, D. V. (1997). Slope stability problems related to glacier shrinkage and permafrost degradation in the Alps. *Eclogae Geologicae Helvetiae*, 90:407–414. 2

Hagg, W., Mayer, C., Lambrecht, A., and Helm, A. (2008). Sub-debris melt rates on Southern Inylchek Glacier, central Tian Shan. *Geografiska Annaler*, 90(1):55–63. 4

Hambrey, M. J., Wuincey, D. J., Glasser, N. F., Reynolds, J. M., Richardson, S. J., and Clemmens, S. (2008). Sedimentological, geomorphological and dynamic context of debris-mantled glaciers, Mount Everest (Sagarmatha) region, Nepal. *Quarternary Science Reviews*, 27(11):2361–2389. 3, 6, 17, 21, 43, 45, 48, 50

Heimsath, A. M. and McGlynn, R. (2008). Quantifying periglacial erosion in the Nepal high Himalaya. *Geomorphology*, 97(1):5–23. 27, 45, 51

Huang, L., Li, Z., Han, H., Tian, B., and Zhou, J. (2018). Analysis of thickness changes and the associated driving factors on a debris-covered glacier in the Tienshan Mountain. *Remote Sensing of Environment*, 206:63–71. 4, 50

Huss, M. and Hock, R. (2015). A new model for global glacier change and sea-level rise. *Frontiers in Earth Science*, 3:1–22. 5

Bibliography

IPCC (2014). Climate change 2014: Synthesis report. contribution of working groups i, ii and iii to the fifth assessment report of the intergovernmental panel on climate change. Technical report, IPCC, Geneva, Switzerland. 2

Jennings, S. J. A., Hambrey, M. J., and Glasser, N. F. (2014). Ice flow-unit influence on glacier structure, debris entrainment and transport. *Earth Surface Processes and Landforms*, 39(10):1279–1292. 21, 22, 50

Juen, M., Mayer, C., Lambrecht, A., Han, H., and Liu, S. (2014). Impact of varying debris cover thickness on ablation: a case study for Koxkar Glacier in the Tien Shan. *The Cryosphere*, 8(2):377–386. 4, 50

Kääb, A., Berthier, E., Nuth, C., Gardelle, J., and Arnaud, Y. (2012). Contrasting patterns of early twenty-first-century glacier mass change in the Himalayas. *Nature*, 488(7412):495–498. 4, 5

Kaser, G., Cogley, J. G., Dyurgerov, M. B., Meier, M. F., and Ohmura, A. (2006). Mass balance of glaciers and ice caps: Consensus estimates for 1961–2004. *Geophysical Research Letters*, 33(19). 5

Kirkbride, M. P. (1993). The temporal significance of transitions from melting to calving termini at glaciers in the central Southern Alps of New Zealand. *The Holocene*, 3(3):232–240. 2, 50

Kirkbride, M. P. (2011). Debris-covered glaciers. In Singh, V. P., Singh, P., and Haritashya, U. K., editors, *Encyclopedia of Snow, Ice and Glaciers*, pages 190–192. Springer. 2, 5

Kirkbride, M. P. and Deline, P. (2013). The formation of supraglacial debris covers by primary dispersal from transverse englacial debris bands. *Earth Surface Processes and Landforms*, 38(15):1779–1792. 2, 5, 7, 44, 49, 50

Kirkbride, M. P. and Warren, C. R. (1999). Tasman Glacier, New Zealand: 20th-century thinning and predicted calving retreat. *Global and Planetary Change*, 22(1):11–28. 3, 49, 50

Konrad, S. K. and Humphrey, N. F. (2000). Steady-state flow model of debris-covered glaciers (rock glaciers). In *Debris-Covered Glaciers: Proceedings of an International Workshop held at the University of Washington in Seattle, Washington, USA, 13-15 September 2000*, pages 255–263. IAHS-AISH Publication. 4, 49

Li, J. and Heap, A. D. (2014). Spatial interpolation methods applied in the environmental sciences: A review. *Environmental Modelling and Software*, 53:173–189. 23

Marzeion, B., Jarosch, A. H., and Gregory, J. M. (2014). Feedbacks and mechanisms affecting the global sensitivity of glaciers to climate change. *The Cryosphere*, 8(1):59–71. 5

Marzeion, B., Jarosch, A. H., and Hofer, M. (2012). Past and future sea-level change from the surface mass balance of glaciers. *The Cryosphere*, 6(6):1295–1322. 5

Matsuoka, N. (2008). Frost weathering and rockwall erosion in the southeastern Swiss Alps: Long-term (1994-2006) observations. *Geomorphology*, 99:353–368. 7, 18

Mattson, L. E. and Gardner, J. S. (1989). Energy exchange and ablation rates on the debris-covered Rakhiot Glacier, Pakistan. *Zeitschrift fÃ¼r Gletscherkunde und Glazialgeologie*, 25:17–32. 4

Mattson, L. E. and Gardner, J. S. (1993). Ablation on debris covered glaciers : an example from the Rakhiot Glacier, Punjab, Himalaya. *Snow and Glacier Hydrology*, 218:289–296. 4

McKinney, D. R. R. D. C. (2014). Debris thickness of glaciers in the Everest area (Nepal Himalaya) derived from satellite imagery using a nonlinear energy balance model. *The Cryosphere*, 8(4):1317–1329. 4, 50

Meier, M. F., Dyurgerov, M. B., Rick, U. K., O'Neel, S., Pfeffer, W. T., Anderson, R. S., Anderson, S. P., and Glazovsky, A. F. (2007). Glaciers dominate eustatic sea-level rise in the 21st century. *Science*, 317(5841):1064–1067. 5

Müller, J., Vieli, A., and Gärtner-Roer, I. (2014). Rockglaciers on the run – Understanding rock-glacier landform evolution and recent changes from numerical flow modeling. *The Cryosphere Discussions*, pages 1–40. 7, 18

Nakawo, M., Iwata, S., Tanabe, O. W., and Yoshida, M. (1986). Processes with distribute supraglacial debris on Khumbu Glacier, Nepal Himalaya. *Annals of Glaciology*, 8(4):129–131. 3, 17, 49, 50

Nakawo, M. and Rana, B. (1999). Estimate of ablation rate of glacier ice under a supraglacial debris layer. *Geografiska Annaler*, 81(4):695–701. 4

Nicholson, L. and Benn, D. I. (2006). Calculating ice melt beneath a debris layer using meteorological data. *Journal of Glaciology*, 52:463–470. 3, 4, 51

Østrem, G. (1959). Ice melting under a thin layer of moraine and the existence of ice cores in moraine ridges. *Geografiska Annaler*, 41(4):228–230. 3, 51

Owen, L. A., Derbyshire, E., and Scott, C. H. (2003). Contemporary sediment production and transfer in high-altitude glaciers. *Sedimentary Geology,*, 155(1):13–36. 4, 50

Pellicciotti, F., Stephan, C., Miles, E., ans W. Immerzeel, S. H., and Bolch, T. (2015). Mass-balance changes of the debris-covered glaciers in the Langtang Himal, Nepal. *Journal of Glaciology*, 61(226):373–386. 4

Post, A. and LaChapelle, E. R. (2000). *Glacier Ice*. University of Washington Press, revised edition edition. 47

Quincey, D. J., Lucas, R. M., Richardson, S. D., Glasser, N. F., Hambrey, M. J., and Reynolds, J. M. (2005). Optical remote sensing techniques in high-mountain environments: applications to glacial hazards. *Progress in Physical Geography*, 29:475–505. 5

Quincey, D. J., Luckman, A., and Benn, D. I. (2009). Quantification of Everest region glacier velocities between 1992 and 2002, using satellite radar interferometry and feature tracking. *Journal of Glaciology*, 55(192):596–606. 4, 49

Bibliography

Radić, V. and Hock, R. (2011). Regionally differentiated contribution of mountain glaciers and ice caps to future sea-level rise. *Nature Geoscience*, 4(2):91–94. 5

Ragettli, S., Bolch, T., and Pellicciotti, F. (2016). Heterogeneous glacier thinning patterns over the last 40 years in Langtang Himal, Nepal. *The Cryosphere*, 10(5):2075–2097. 4

Raper, S. C. B. and Braithwaite, R. J. (2006). Low sea level rise projections from mountain glaciers and icecaps under global warming. *Nature*, 439(7074):311–313. 5

Reid, T. D. and Brock, B. W. (2010). An energy-balance model for debris-covered glaciers including heat conduction through the debris layer. *Journal of Glaciology*, 56(199):903–916. 4

Rogerson, P. A. (2015). *Statistical methods for geography.* SAGE Publications, 4th edition edition. 25, 26

Rounce, D. R., Quincey, D. J., and McKinney, D. C. (2015). Debris-covered glacier energy balance model for Imja-Lhotse Shar Glacier in the Everest region of Nepal. *The Cryosphere*, 9(6):2295–2310. 5

Rowan, A. V., L., E. D., Quincey, D. J., and F., G. N. (2015). Modelling the feedbacks between mass balance, ice flow and debris transport to predict the response to climate change of debris-covered glaciers in the Himalaya. *Earth and Planetary Science Letters*, 430:427–438. 5

Schauwecker, S., Rohrer, M., Huggel, C., Kulkarni, A., Ramanathan, A. L., Salzmann, N., Stoffel, M., and Brock, B. (2015). Remotely sensed debris thickness mapping of Bara Shigri Glacier, Indian Himalaya. *Journal of Glaciology*, 61(228):675–688. 4, 5, 50

Scherler, D., Bookhagen, B., and Strecker, M. R. (2011). Spatially variable response of Himalayan glaciers to climate change affected by debris cover. *Nature Geoscience*, 4:156–159. 4, 5, 6, 45, 49

Setianto, A. and Triandini, T. (2013). Comparison of kriging and inverse distance weighted (IDW) interpolation methods in lineament extraction and analysis. *Journal of Southeast Asian Applied Geology*, 5(1):21–29. 23

SLF (2017). *Institut für Schnee und Lawinenforschung: RAMMS::AVALANCHE User Manual.* 20, 47

swisstopo (2018). Bundesamt für Landestopographie. 10, 15, 16, 45, 49

UZH (2018). University of Zurich: Methodenberatung. `https://www.methodenberatung.uzh.ch/de.html`. Accessed: 25.05.2018. 25, 26

Wang, P., Li, Z., Li, H., Wang, W., Zhou, P., and Wang, L. (2017). Characteristics of a partially debris-covered glacier and its response to atmospheric warming in Mt. Tomor, Tien Shan, China. *Global and Planetary Change*, 159:11–24. 4, 50

WGMS (2017). Global glacier change bulletin no. 2 (2014-2015). Technical report, ICSU(WDS)/IUGG(IACS)/UNEP/UNESCO/WMO, World Glacier Monitoring Service, Zurich, Switzerland. 2, 9

Zhang, Y., Fujita, K., Liu, S., Liu, Q., and Nuimura, T. (2011). Distribution of debris thickness and its effect on ice melt at Hailuogou glacier, southeastern Tibetian Plateau, using in situ surveys and ASTER imagery. *Journal of Glaciology*, 57(206):1147–1157. 5, 50

A. Raster Data
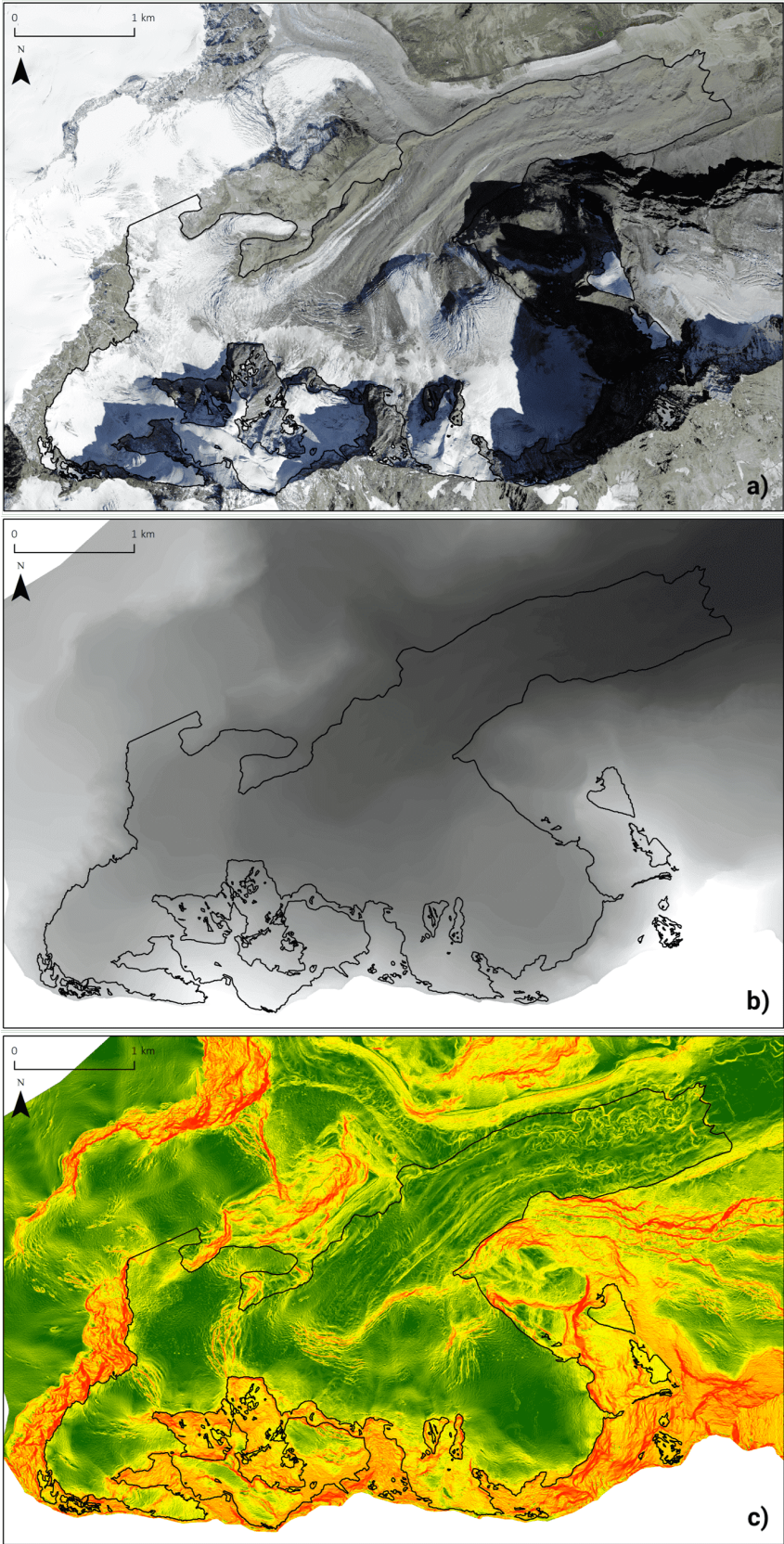
Figure A.1. Raster data for Zmuttgletscher. a) Orthophotograph from 2010. b) DTM from 2010. c) Slope raster from 2010. The outlines of Zmuttgletscher are given in black.

B. Velocity Data
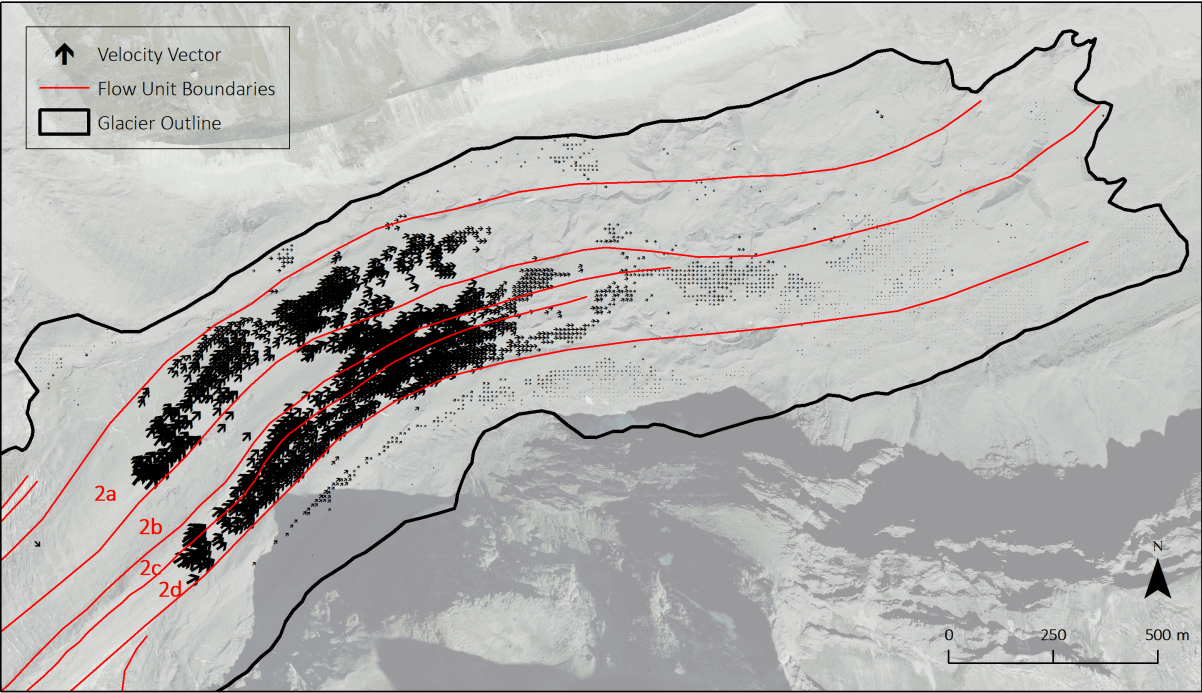
Figure B.1. Velocity vectors on ablation area of Zmuttgletscher. The length and direction of the black vector arrows shows the surface displacement per year between 2016 and 2017 (Mölg et al., in prep.). The labels mark the respective flow subunits.

C. Maps
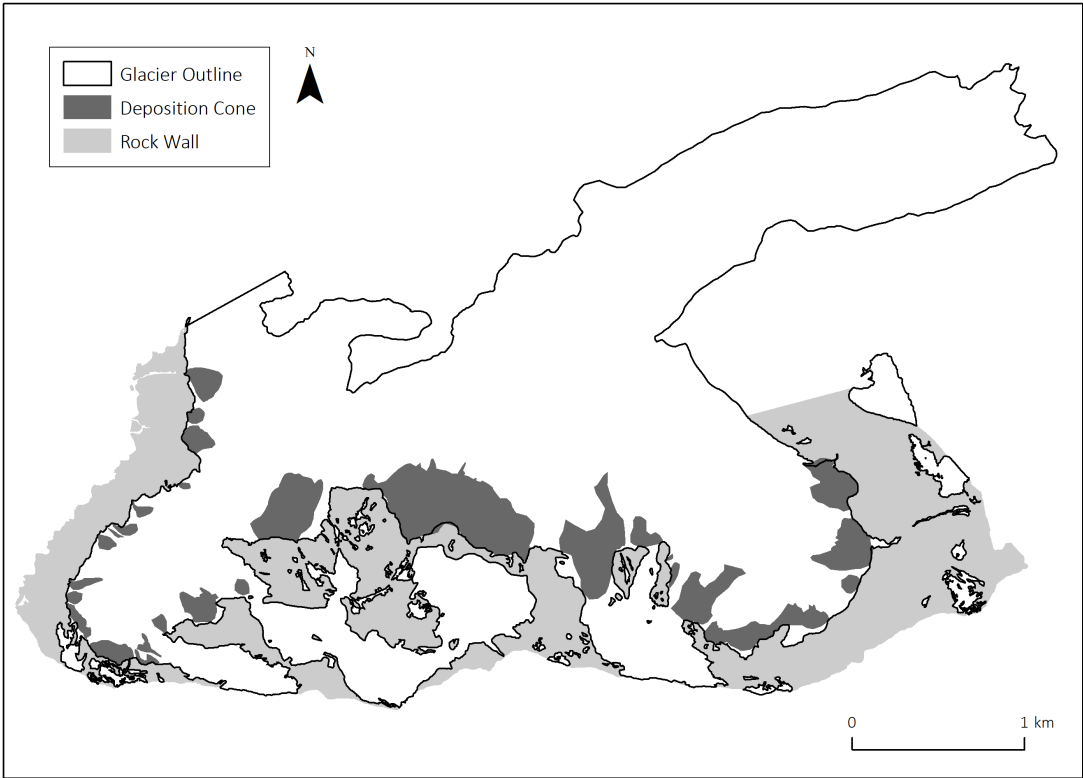
Figure C.1. Mapped rock walls and mapped deposition cones.
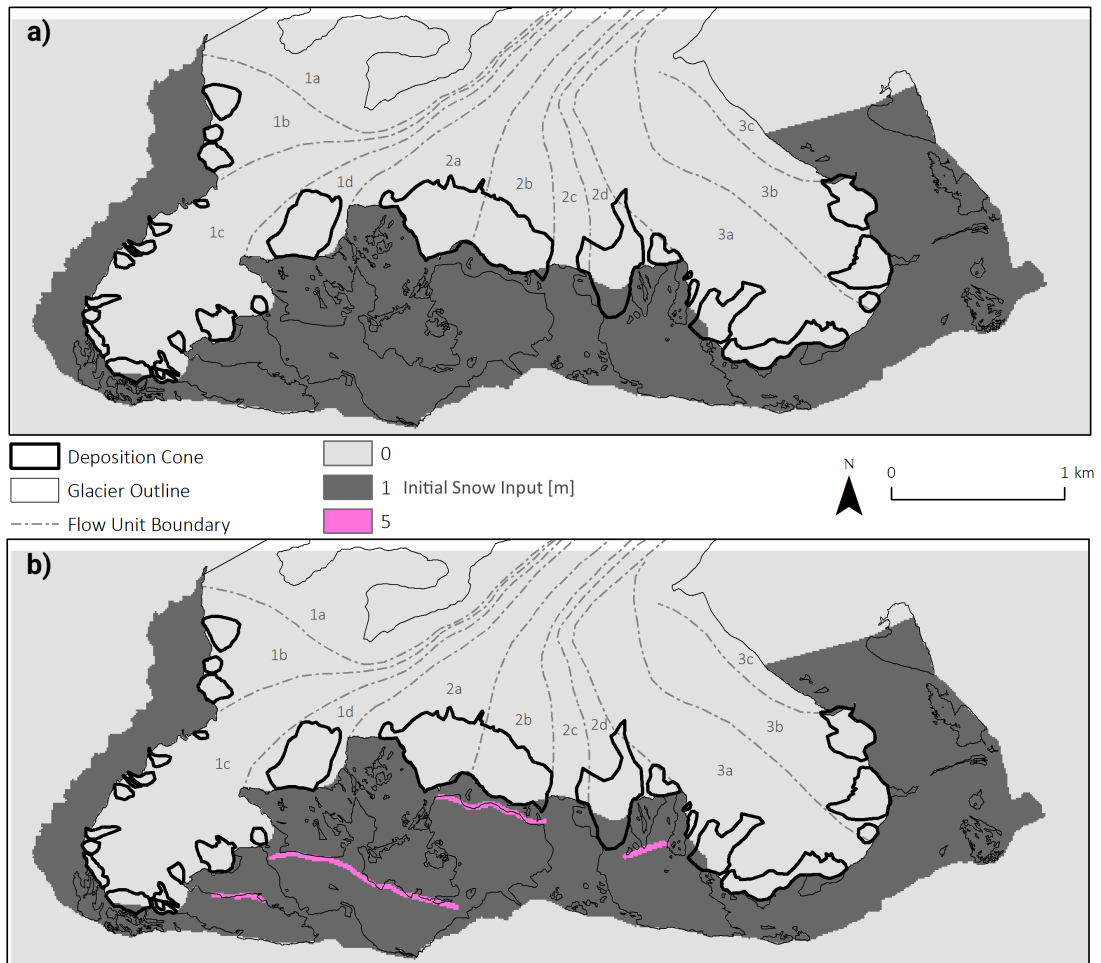
Figure C.2. Snow input for the MTD sensitivity analysis. The labels mark the respective flow subunit. a) Constant snow input $I = 1m$ for the headwall pixels, b) Snow input $I = 5m$ for the hanging glacier calving front pixels and $I = 1m$ for the remaining headwall pixels.

C. Maps

Declaration of Originality

I hereby declare that the submitted thesis is the result of my own, independent work. All external sources are explicitly acknowledged in the thesis.

Zurich, 30th September 2018 ⸺⸺⸺⸺⸺⸺⸺⸺⸺⸺